Electromagnetic Pinned Solitons for Space Debris Detection

Abhijit Sen,[1, a)] Rupak Mukherjee,[2, 3] Sharad K. Yadav,[4] Chris Crabtree,[5] and Gurudas Ganguli[5]

[1)] *Institute for Plasma Research, Bhat, Gandhinagar 382428, India*

[2)] *Department of Physics, School of Physical Sciences, Sikkim University, Gangtok, Sikkim, 737102, India*

[3)] *Princeton Plasma Physics Laboratory, Princeton, N.J. 08536, U.S.A.*

[4)] *Department of Physics, S.V.N.I.T. Surat, Surat 395007, India.*

[5)] *Naval Research Laboratory, Washington, DC 20375, U.S.A.*

(Dated: 3 December 2022)

Electromagnetic "pinned" solitons in the form of stationary nonlinear waves are studied within the framework of an inertial magneto-hydrodynamic model. These structures that can arise when a charged source moves in a magnetized plasma have a velocity that is equal to the source velocity and hence appear as "pinned" structures that envelope the source. We investigate the excitation of such solitons in the Low Earth Orbit (LEO) region due to the passage of charged orbital debris objects. The spatial size of these electromagnetic solitons, typically of the order of a few ion skin depths, can be very large in this region. Such solitons can be detected using a variety of ground-based or orbit based radio sounding techniques and may provide a convenient additional means of tracking small sized orbital debris objects that are difficult to spot optically.

[a)]Electronic mail: senabhijit@gmail.com

I. INTRODUCTION

The population of 'space debris' also known as 'space junk' or 'orbital debris' consisting of dead or destroyed satellites, their fragmented parts, rocket bodies and mission related debris continues to grow at an alarming rate thereby posing a serious threat to active space assets[1]. Space debris concerns have delayed mission launches and space walks by astronauts. It is estimated that at the present time there are over half a million pieces of debris with sizes ranging from 1 to 10 cms and nearly 100 million particles that are less than a centimetre orbiting the earth[2–4]. The majority of the debris population resides in the region between 600 kms to 1200 kms altitude in sun-synchronous Low Earth Orbit (LEO) region where they pose the greatest threat to the high population of active orbiting space craft[1]. Since the debris objects have a high orbital velocity (of the order of 8 kms/s in the LEO region) even a small centimetre sized particle has tremendous kinetic energy and can cause enormous damage if it collides with a satellite[5]. According to NASA, a collision with even a millimeter-size debris at orbital speed can be mission ending[6]. Individual small sized objects are difficult to detect using optical techniques or even directly by radar scatterings. Therefore, modelling the dynamics of these objects and devising better methods of detecting them remain a high priority research area of Space Situational Awareness[7,8].

An important physical characteristic of the space debris is that they are highly charged objects. This is because they are moving in the space plasma environment of the ionosphere and the flow of electron and ion currents on them can lead to the accumulation of a large amount of surface charge (usually negative) and the development of a surface potential on these objects[9,10]. For a moving object like a debris the charging time can be slightly increased depending on the speed[11]. However, since the charging time is significantly smaller than the residence time of the debris in the plasma, the debris speed is not relevant to our present investigation. For our analysis we assume that the charge on the debris has already reached a steady state. The charged debris are subject to electromagnetic forces from the surrounding plasma and the ambient magnetic field[10] and in turn can also excite electromagnetic perturbations in the plasma[12]. While the electromagnetic forces acting on the debris have been investigated in detail and found to be negligible to affect orbital motion compared to other primary forces like gravity[10], the consequences of the charge interactions

with the ambient plasma leading to electromagnetic emissions by the debris have not received much attention. In a series of investigations, we examined this topic and suggested an alternate way of tracking small sized debris by exploiting these collective perturbations induced by them in the plasma[12–15]. The basic idea is that these nonlinear excitations, which take the form of long-lived soliton structures and travel ahead of the debris object, can give rise to a cloud of plasma irregularity with a dimension much larger than the debris size. Such irregularities can be detected from ground or space based radars and thereby provide an indirect means of detecting the debris object. This theoretical idea of the possibility of exciting a precursor soliton in a plasma was confirmed experimentally in a laboratory device using a flowing dusty plasma interacting with a static charged obstacle[13]. It was shown that when the magnitude of the flow exceeded a critical value (in this case the dust acoustic speed) precursor pulses were created in addition to the customary trailing wake fields. The pulses were analysed for their propagation characteristics and found to be fast propagating dust acoustic solitons. Subsequent experiments also explored the nature of these solitons as a function of the size and shape of the charged obstacle[16]. In a detailed feasibility study, Truitt and Hartzell[17–19] have worked out the amplitude, width, and production frequency of ion acoustic solitons that may be produced by millimeter and centimeter-scale orbital debris as a function of the debris' size, velocity, and location (altitude, latitude, and longitude) about the Earth. Finally, another class of solitons, also theoretically predicted earlier[12], was identified in a dusty plasma experiment[20]. These solitons do not move away from the source but cling to it as an envelope forming an electric sheath around it and are known as "pinned" solitons. Typically, the envelope can be quite large compared to the normal Debye shield around the source and could again provide a means of detecting the debris using radar scattering.

All these past works[12–17,20] were confined to electrostatic excitations *e.g.* ion acoustic waves or dust acoustic waves which are easy to model theoretically and also test experimentally. Ion acoustic waves excited by the debris in the ionosphere are likely to have short lifetimes due to Landau damping effects particularly in the LEO region where the electron and ion temperatures are nearly equal[21,22]. Although ion Landau damping can be eliminated by an inhomogeneous ion flow[23], that can arise from a speeding debris, a better alternative would be to excite electromagnetic waves which would not suffer such damping and can be longer lived. Electromagnetic solitons would also have a larger spatial extent, of the order

of a few ion skin depths, and would be easier to detect with radar back scattering. Since a moving charge constitutes a current, the orbiting debris can be seen as current sources and hence, in principle, should be able to emit electromagnetic waves. In the presence of an ambient magnetic field these could be in the form of Alfven waves or magnetosonic waves[24,25]. However there still remains the question of whether they can emit electromagnetic precursor waves and what would be their characteristics. The question was addressed in Kumar and Sen[26] where particle-in-cell simulations provided a first principles proof of existence of driven electromagnetic solitons. It was shown that a charge bunch moving in a magnetized plasma could excite precursor waves in the form of fast magneto-sonic solitons. Under other conditions, the simulations also observed the existence of fast magneto-sonic pinned solitons. While the PIC simulations have helped establish the existence of electromagnetic precursor solitons, for information about their spectrum and physical characteristics a fluid simulation is more convenient and provides good physical insights[27,28]. The present paper is devoted to such an investigation where we look for a wide class of driven nonlinear stationary solutions of the magneto-hydrodynamic set of equations. We pay special attention to pinned solitons which move at the same speed as the charge source (the orbital debris object) and discuss their propagation characteristics. Our results are primarily numerical but we also discuss analytic solutions and reduced nonlinear models in certain simplifying limits. Finally we discuss the relevance and applicability of our results to the debris detection problem in the LEO region.

The paper is organized as follows. The next section, section II, is devoted to a description of the model equations as well as the equilibrium configuration and parameters. Section III provides a reduced nonlinear model in the form of a forced Korteweg de Vries (fKdV) equation that is derived (in Appendix A) from the full model equations by employing a reductive perturbation method. Some analytic and numerical results of the fKdV are presented. Section IV presents nonlinear stationary solutions for arbitrary amplitudes in various regimes through numerical solutions of the full set of model equations in the frame of the moving source. In section V we discuss the physical significance of our solutions and their relevance and applicability to the debris detection problem.

II. MODEL EQUATIONS

Our model equations are derived from the standard two fluid model equations[24,25], by making the MHD approximation of quasi-neutrality ($n_e = n_i = n$) and defining the mass $M_{ei} = m_e + m_i \approx m_i$ and the MHD fluid velocity as, $\vec{v} = \frac{m_i}{M_{ei}}\vec{v}_i + \frac{m_e}{M_{ei}}\vec{v}_e \approx \vec{v}_i$. Here $m_j, n_j, \vec{v}_j$ refer to the two fluid electron ($j = e$) and ion ($j = i$) quantities.

Then the continuity equation is given by,

$$\frac{\partial n}{\partial t} + \nabla \cdot (n\vec{v}) = 0 \tag{1}$$

By adding the electron and ion momentum equations, one gets the following MHD momentum equation,

$$\frac{d\vec{v}}{dt} = \frac{1}{M_{ei}nc}\vec{J} \times \vec{B} - \frac{1}{nM_{ei}}\nabla p \tag{2}$$

where $\vec{J} = en(\vec{v}_i - \vec{v}_e)$ and $p = n(T_e + T_i)$. To account for the effect of the moving charged debris source we introduce an additional current source $\vec{S}$ in the Ampere's law which is now given by,

$$\nabla \times \vec{B} = \frac{4\pi}{c}\vec{J} + \vec{S} \tag{3}$$

Finally, we have Faraday's law,

$$\frac{\partial \vec{B}}{\partial t} = -\nabla \times \vec{E} \tag{4}$$

Using eq. (3) to substitute for $\vec{J}$ in eq. (2) we get

$$\frac{d\vec{v}}{dt} = \frac{1}{4\pi nM_{ei}}(\nabla \times \vec{B}) \times \vec{B} - \frac{1}{4\pi nM_{ei}}\vec{S} \times \vec{B} + \frac{1}{nM_{ei}}\nabla(p) \tag{5}$$

The electric field is calculated from the ion momentum equation to get,

$$\begin{aligned} \vec{E} &= -\frac{1}{c}\vec{v}_i \times \vec{B} + \frac{m_i}{e}\frac{dv_i}{dt} \\ &\approx -\frac{1}{c}\vec{v} \times \vec{B} + \frac{M_{ei}}{e}\frac{dv_i}{dt} \end{aligned} \tag{6}$$

Substituting for $\vec{E}$ in Faraday's law one gets,

$$\frac{\partial \vec{B}}{\partial t} = \nabla \times \left(\vec{v} \times \vec{B}\right) - \frac{M_{ei}c}{e}\nabla \times \frac{d\vec{v}}{dt} \tag{7}$$

The last term in eq.(2) comes from retaining the ion inertial contribution and provides a dispersive contribution. Equations (1),(2) and (7) constitute our full set of model equations.

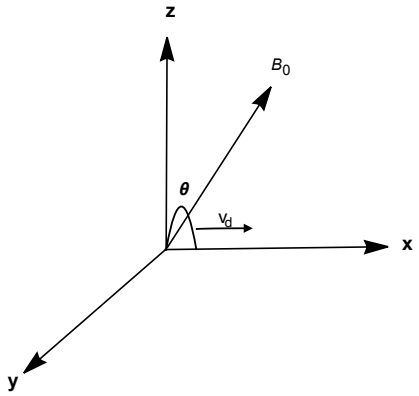

FIG. 1: Configuration of the equilibrium magnetic field with respect to the orbital debris propagation direction. The initial position and velocity direction of the debris object are shown in a cartoon form in the figure.

We next assume that the debris is moving in the x direction ($\vec{S} = S\hat{e}_x$) and thus only consider perturbations with x variation. We take the equilibrium magnetic field to be $\mathbf{B_0} = B_{0x}\hat{e}_x + B_{0z}\hat{e}_z$ with $B_{0x} = B_0 sin\theta$ and $B_{0z} = B_0 cos\theta$ where θ is the angle between the magnetic field and z, the direction perpendicular to the direction of the wave propagation (see Fig.1). We now write eqns.(1), (2) and (7) in component form and further use the following normalizations,

$$x = \frac{x}{\delta} \; ; \; t = \frac{tV_A}{\delta}$$

$$n = n/n_0 \; ; \; \vec{v} = \vec{v}/V_A \; ; \; \vec{B} = \vec{B}/B_0$$

where $\delta = \frac{c}{\omega_{pi}}$ is the ion skin depth, $V_A = \frac{B_0}{\sqrt{4\pi n_0 m_i}}$ is the Alfven velocity and $\omega_{pi} = \sqrt{4\pi n_0 e^2/m_i}$ is the ion plasma frequency. The normalized set of evolution equations are

then given by,

$$\frac{\partial n}{\partial t} + \frac{\partial}{\partial x}\left(n v_x\right) = 0 \tag{8}$$

$$\frac{\partial v_x}{\partial t} + v_x \frac{\partial v_x}{\partial x} = -\frac{1}{2n}\frac{\partial}{\partial x}\left((b_z + \cos(\theta))^2 + b_y^2\right) - \frac{\beta}{n}\frac{\partial n}{\partial x} \tag{9}$$

$$\frac{\partial v_y}{\partial t} + v_x \frac{\partial v_y}{\partial x} = \frac{1}{n}\sin\theta \frac{\partial b_y}{\partial x} + \frac{S}{n}(\cos(\theta) + b_z) \tag{10}$$

$$\frac{\partial v_z}{\partial t} + v_x \frac{\partial v_z}{\partial x} = \frac{1}{n}\sin\theta \frac{\partial b_z}{\partial x} - \frac{S}{n} b_y \tag{11}$$

$$\frac{\partial b_y}{\partial t} = -\frac{\partial}{\partial x}(v_x b_y - v_y \sin\theta) + \frac{\partial}{\partial x}(\frac{1}{n}\sin\theta \frac{\partial b_z}{\partial x} - \frac{S b_y}{n}) \tag{12}$$

$$\frac{\partial b_z}{\partial t} = \frac{\partial}{\partial x}\left(v_z \sin\theta - v_x(\cos\theta + B_z)\right) - \frac{\partial}{\partial x}\left(\frac{1}{n}\sin\theta \frac{\partial b_y}{\partial x} + \frac{S}{n}(\cos(\theta) + b_z)\right) \tag{13}$$

where $\beta = C_s^2/V_A^2$ with $C_s = \sqrt{T/m_i}$ being the sound velocity. Furthermore, b_y, b_z denote perturbed magnetic field components and $b_x = 0$ follows from the x component of Faraday's law.

For $S = 0$, linearising the above equations and taking the linear quantities to be of the form $\tilde{f} \sim \exp(-i\omega t + ikx)$, one gets the following dispersion relation[24]:

$$M_1^6 - M_1^4(1 + \sin^2\theta + k^2\delta^2 \sin^2\theta + \beta) + M_1^2 \sin^2\theta \left(1 + \beta(2 - k^2\delta^2)\right) - \beta \sin^4\theta = 0 \tag{14}$$

where $M_1 = \omega/kV_A$. The above dispersion relation can be solved to obtain the full spectrum of MHD waves including the Alfven waves and the fast and slow magneto-sonic waves. The $k^2\delta^2$ term in eq. (14) is the ion inertia contribution and provides the essential dispersion contribution for the formation of a soliton for very low frequency waves in the cold plasma limit. We will discuss these waves in the context of applications to the LEO region.

III. SMALL AMPLITUDE NONLINEAR SOLUTIONS - THE FKDV LIMIT

Before attempting to solve the full set of model equations for arbitrary amplitudes of the variables, we first discuss a reduced model equation that can be obtained from eqns. (8-13) in the limit of weak nonlinearity (small but finite amplitude perturbations) and weak dispersion. This leads to a nonlinear evolution equation in the form of a forced Korteweg de Vries (fKdV)[29,30] equation which is easier to analyze than the full set of model equations. A

systematic derivation of such an equation using the reductive perturbation method is given in the Appendix. The equation is,

$$a_1\frac{\partial b_{z1}}{\partial \tau} + a_2 b_{z1}\frac{\partial b_{z1}}{\partial \xi} + a_3\frac{\partial^3 b_{z1}}{\partial \xi^3} = a_4\frac{\partial S_2}{\partial \xi} \tag{15}$$

where, $\xi = \epsilon^{1/2}(x - ut)$ is the stretched variable in the wave frame moving with velocity u, $\tau = \epsilon^{3/2}t$ is a stretched time describing the temporal evolution of the perturbed quantities in the wave frame and ϵ is the expansion parameter. b_{z1} is the first order perturbed variation in the z component of the wave magnetic field and S_2 is the source term which is assumed to be an order higher than the field perturbations. M the Mach number is defined as $M = u/V_A$ and the coefficients a_n are defined as,

$$a_1 = (\beta + M^2)\cos(\theta) - \frac{(\beta - M^2)((M-\beta)}{M}\sin(\theta)\tan(\theta) + \frac{M(M^2-\beta)(M-\beta)}{\cos(\theta)}$$

$$a_2 = 2\frac{\beta}{M-\beta}\cos^2(\theta) + \left(1 - M + \frac{(M-\beta)^2}{\cos^2(\theta)}\right)\frac{M^2}{M-\beta}\cos^2(\theta) + \frac{(M^2-\beta)(1-M)}{M}\sin^2(\theta)$$
$$+2M(M^2-\beta)$$

$$a_3 = -\frac{(M^2-\beta)(M-\beta)M^2\tan(\theta)\sin(\theta)}{(M^2 - \sin^2(\theta))}$$

$$a_4 = M - \beta$$

A similar fKdV equation had earlier been derived for the electrostatic case by Sen *et. al.*[12] to model the excitation of ion acoustic precursor solitons by a charged debris object. The above eq.(15) models electromagnetic emissions from a moving charged debris and like the electrostatic case can produce both precursor solitons as well as pinned solitons. For the case of pinned solitons eq.(15) has some exact analytic solutions[12] for particular forms of S_2. For example if,

$$S_2 = AB\text{sech}^2\left[\sqrt{\frac{Aa_2}{12a_3}}\left(\xi - \frac{Aa_2 - 3Ba_4}{3a_1}\tau\right)\right]$$

then a solution of eq. (15) is

$$b_{z1} = A\text{sech}^2\left[\sqrt{\frac{Aa_2}{12a_3}}\left(\xi - \frac{Aa_2 - 3Ba_4}{3a_1}\tau\right)\right]$$

where A and B are constants. Typically $B \ll 1$, since in this approximation the source perturbation is taken to be small. The amplitude of the soliton is larger than the source

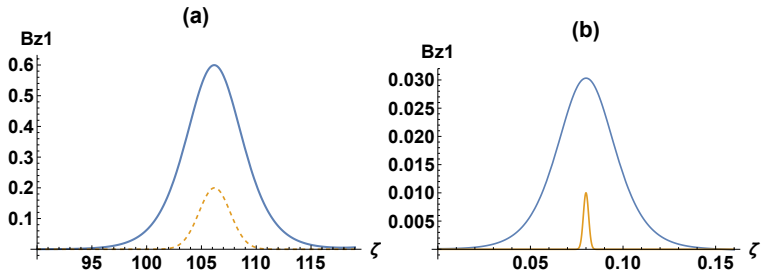

FIG. 2: (a)Pinned soliton of (17) for M=0.25, $\beta = 1.6$, $A_0 = 0.001$, $\Delta = 2.0$, propagating at an angle $\theta = 15^0$. In the plot the amplitude of the source has been multiplied by a factor of 200 to make it visible in the chosen scale and is given by a dashed orange line. (b)Pinned soliton of (17) for M=0.01, $\beta = 0$, $A_0 = 1. * 10^{-7}$,$\Delta = 0.002$ and $\theta = 2.59$. The amplitude of the source has been multiplied by a factor of 10^5 to make it visible in the chosen scale of the plot and is given by a solid orange line.

by a factor of $1/B$. In other words, the source is enveloped by an electromagnetic structure that is much larger than the source size. For arbitrary forms of the source one can look for pinned soliton solutions of eq.(15) by looking for stationary solutions in a frame where the source travels at the same speed as the soliton. Taking the normalised frame speed to be M and going to the frame defined by $\zeta = \xi - M\tau$ one can convert eq. (15) to,

$$-Ma_1\frac{\partial b_{z1}}{\partial \zeta} + a_2 b_{z1}\frac{\partial b_{z1}}{\partial \zeta} + a_3\frac{\partial^3 b_{z1}}{\partial \zeta^3} = a_4\frac{\partial S_2}{\partial \zeta} \tag{16}$$

This equation can be integrated once to give,

$$a_3\frac{\partial^2 b_{z1}}{\partial \zeta^2} + a_2\frac{b_{z1}^2}{2} - Ma_1 b_{z1} = a_4 S_2 \tag{17}$$

where we have used the condition that b_{z1} and its derivatives vanish at infinity for soliton solutions. Eqn.(17) can be solved numerically for arbitrary functional forms of S_2. Fig.2 shows some typical soliton solutions for a Gaussian current source,

$$S_2 = A_0 e^{\frac{(\zeta-\zeta_0)^2}{\Delta^2}}$$

with amplitude A_0 and width Δ. The plot in Fig. 2 (a) shows a slow magneto-sonic soliton with $\beta = 1.6$ and $M = 0.25$. Fig. 2(b) shows a much slower ion inertial wave soliton with $\beta = 0$ and $M = 0.01$. As we will discuss later, pinned solitons belonging to the inertial

wave branch are likely to be excited in the LEO region since their velocities match with those of the orbital debris objects in that region. In both the figures it can be seen that the source is enveloped by a soliton that is several times larger in amplitude. For obtaining our numerical solutions, we have used a Fourth order Runge Kutta numerical integrator to solve ODEs in the wave frame and a pseudo-spectral method to solve PDEs for time evolution of the pinned solitons. To evaluate the Fourier transform, we have used the FFTW library (version 3.3.8). For each individual case, the grid resolution and time step width have been chosen to satisfy the CFL (Courant–Friedrichs–Lewy) condition[31].

IV. NONLINEAR STATIONARY SOLUTIONS FOR ARBITRARY AMPLITUDES

For arbitrary amplitude solitons we look for stationary solutions of the full set of nonlinear equations (8-13). To get an idea of the basic nature and spectrum of the solitons we first turn off the source term ($S = 0$) and also take $\beta = 0$ to look for the existence of nonlinear stationary solutions for the above equations.

A. Alfvenic and Ion Inertial Wave Solitons ($S = 0$, $\beta = 0$)

As in the KdV case, we convert the partial differential equations (8-13) to ordinary differential equations by transforming to the frame $\zeta = x - Mt$ where M is the normalized velocity of the soliton.

$$-M\frac{\partial n}{\partial \zeta} + \frac{\partial}{\partial \zeta}\left(n v_x\right) = 0 \tag{18}$$

$$(-M + v_x)\frac{\partial v_x}{\partial \zeta} = -\frac{1}{2n}\frac{\partial}{\partial \zeta}\left((\cos(\theta) + b_z)^2 + b_y^2\right) \tag{19}$$

$$(-M + v_x)\frac{\partial v_y}{\partial \zeta} = \frac{1}{n}\sin(\theta)\frac{\partial b_y}{\partial \zeta} \tag{20}$$

$$(-M + v_x)\frac{\partial v_z}{\partial \zeta} = \frac{1}{n}\sin(\theta)\frac{\partial b_z}{\partial \zeta} \tag{21}$$

$$-M\frac{\partial b_y}{\partial \zeta} = -\frac{\partial}{\partial \zeta}(v_x b_y - v_y \sin(\theta)) + \frac{\partial}{\partial \zeta}(\frac{1}{n}\sin(\theta)\frac{\partial b_z}{\partial \zeta}) \tag{22}$$

$$-M\frac{\partial b_z}{\partial \zeta} = \frac{\partial}{\partial \zeta}\left(v_z \sin(\theta) - v_x(\cos(\theta) + b_z)\right)) - \frac{\partial}{\partial \zeta}(\frac{1}{n}\sin(\theta)\frac{\partial b_y}{\partial \zeta}) \tag{23}$$

Integrating eq. 18) once and using the asymptotic condition $n \to 1$; $v_x \to 0$ as $\zeta \to \infty$ we get

$$n(M - v_x) = M \tag{24}$$

Using eq. 24) in eq. (19) we can get,

$$Mv_x = \frac{1}{2}\left(b^2 + 2\cos(\theta)b_z\right) \tag{25}$$

where we have used the conditions $b_y \to 0$ as $\zeta \to \infty$. Also $b^2 = b_y^2 + b_z^2$. In like fashion, from eq.(20) and eq.(21), we can get,

$$Mv_y = -\sin(\theta)b_y \tag{26}$$

$$Mv_z = -\sin(\theta)b_z \tag{27}$$

From eq. (22) and eq. (23) we get,

$$-Mb_y = \sin(\theta)(nv_y + \frac{\partial b_z}{\partial \zeta}) \tag{28}$$

$$-Mb_z = \sin(\theta)(nv_z - \frac{\partial b_y}{\partial \zeta}) - nv_x\cos(\theta) \tag{29}$$

Substituting for v_y, v_z and v_x in eq. (28) and eq. (29) we get,

$$\sin(\theta)\frac{\partial b_z}{\partial \zeta} + \left(M - n\frac{\sin^2(\theta)}{M}\right)b_y = 0 \tag{30}$$

$$\sin(\theta)\frac{\partial b_y}{\partial \zeta} - \left(M - n\frac{\sin^2(\theta)}{M}\right)b_z + \frac{n\cos\theta(b^2 + 2\cos(\theta)b_z)}{2M} = 0 \tag{31}$$

From eq.(24) and eq. (25) we can get,

$$n = \frac{2M^2}{2M^2 - b^2 - 2\cos(\theta)b_z} \tag{32}$$

Substituting for n in eq. (30) and eq. (31) we get the following two coupled equations for b_y and b_z.

$$M\sin(\theta)\frac{\partial b_z}{\partial \zeta} + \left(M^2 - \frac{2M^2\sin^2(\theta)}{2M^2 - b^2 - 2\cos(\theta)b_z}\right)b_y = 0 \tag{33}$$

$$M\sin(\theta)\frac{\partial b_y}{\partial \zeta} - \left(M^2 - \frac{2M^2\sin^2(\theta)}{2M^2 - b^2 - 2\cos(\theta)b_z}\right)b_z + \frac{M^2\cos(\theta)(b^2 + 2\cos(\theta)b_z)}{2M^2 - b^2 - 2\cos(\theta)b_z} = 0 \tag{34}$$

Similar equations have been derived and discussed earlier[32,33] in the context of low frequency nonlinear stationary waves in a magnetised plasma. Some typical solitonic solutions

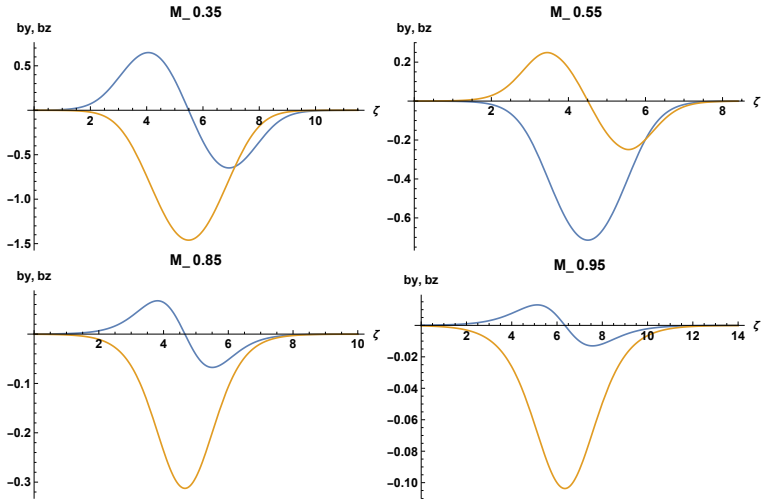

FIG. 3: Alfvenic solitons for different values of $M < 1$ and $\theta = 15^0$. The unipolar curves (orange) are of b_z and the dipolar curves (blue) are of b_y.

of the above equations for different values of M and a chosen θ are shown in Fig. 3. These solutions have a similarity with the solitary wave solutions obtained by Adlam and Allen[34,35] who considered nonlinear hydromagnetic waves generated by rapid compression of a magnetised plasma.

Our numerical investigations show that these solitons, which are pure Alfvenic solitons (since $\beta = 0$), only exist for $M < 1$. As $M \to 1$, their amplitude decreases very rapidly and then they cease to exist. One requires a finite β to have soliton solutions for $M > 1$. These are discussed in the next subsection IV B.

To test whether the arbitrary amplitude stationary solutions are also solutions of the full set of fluid Eqs. (8-13) one can use them as initial conditions and see whether they propagate. In Fig.4 we show the time evolution of the soliton obtained for $M = 0.35$ at $\theta = 15°$. As can be seen, the solution evolves in time without distortion suggesting that these exact time stationary numerical solutions are indeed also solutions of the full plasma system. They can thus be excited by an external driving term such as a charged debris to form a pinned soliton.

As one approaches the small M limit the existence region of ion inertial wave solitons is

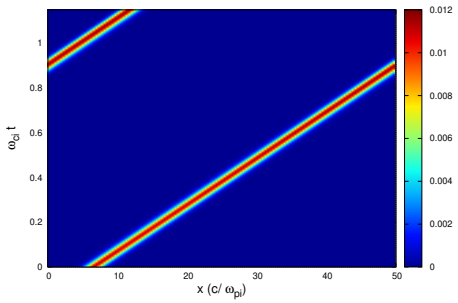

FIG. 4: Plot showing the time evolution of the soliton solution with M=0.95 obtained by simultaneously solving eqns. (8-13) using the solution of eqns. (33) and (34) as an initial condition. The intensity plot shows the profile of B_z^2. As can be seen the soliton propagates without distortion.

strongly influenced by θ, the angle of propagation[32,33]. For a given angle of propagation, soliton solutions cease to exist below a certain value of M. Solitons with very low values of M exist for very small values[32,33] of θ. Fig. 5 shows some of these typical low M solitons.

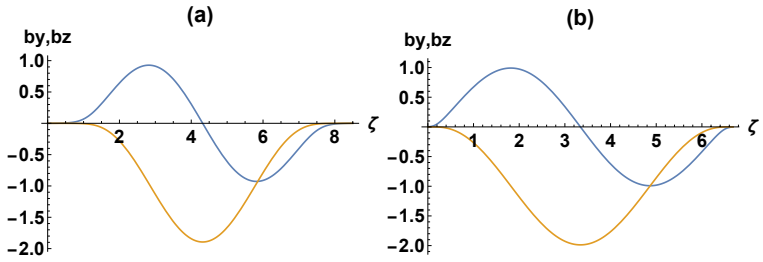

FIG. 5: Ion inertial wave solitons for (a) $M = 0.1$, $\beta = 0$, $\theta = 5^0$ and (b) $M = 0.0185$, $\beta = 0$ and $\theta = 1^0$. The unipolar curves (orange) are of b_z and the dipolar curves (blue) are of b_y.

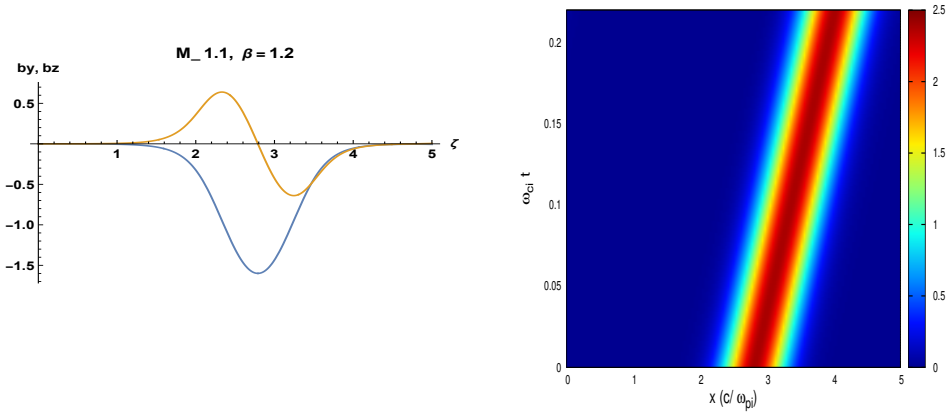

(a) (b)

FIG. 6: (a) Magnetosonic soliton at $M = 1.1$, $\beta = 1.2$. The unipolar curve (blue) is of b_z and the dipolar curve (orange) is of b_y. (b) Time evolution of this soliton shown in terms of b_z^2. This is obtained by simultaneously solving eqns. (8-13), with the initial condition taken from the solution of eqns. (30, 31) and eqn. (37)

B. Magnetosonic Solitons ($S = 0$, β finite)

We now consider finite β effects that allow for the existence of magnetosonic waves. With finite β, eqn(19) becomes,

$$(-M + v_x)\frac{\partial v_x}{\partial \zeta} = -\frac{1}{2n}\frac{\partial}{\partial \zeta}\left((\cos(\theta) + b_z)^2 + b_y^2\right) - \frac{\beta}{n}\frac{\partial n}{\partial \zeta} \tag{35}$$

Integrating once we get,

$$M v_x = \frac{(b^2 + 2\cos(\theta) b_z)}{2} + \beta(n-1) \tag{36}$$

Eliminating v_x between (24) and (36) one gets a quadratic equation for n whose solutions are,

$$n_\pm = \frac{2M^2 + 2\beta - C \pm \sqrt{(2\beta + 2M^2 - C)^2 - 16M^2\beta}}{2\beta} \tag{37}$$

where $C = (b^2 + 2\cos(\theta)b_z)$. Note that the limit of $\beta \to 0$ is singular in the above expression for the density. We can arrive at a proper expression for n in that limit by applying L'H$\hat{o}$pital's rule, namely, taking the limit of the ratio of the derivative of the numerator and the derivative of the denominator w.r.t β and then taking the limit of $\beta \to 0$. The choice of n_+ gives the correct expression for n for $\beta = 0$, namely, eqn.(32).

In Fig.6(a) we show a magnetosonic soliton solution for $M = 1.1$, $\beta = 1.2$ by solving eqns.(30) and (31) with the expression for n_+ given in (37). The time evolution of such a soliton when used as an initial condition in the full set of equations is shown in Fig.6(b).

C. Pinned Solitons of Ion Inertial Waves (S finite, $\beta = 0$)

Our ultimate aim is to excite pinned solitons that envelope a driving current source. For this we need to look for stationary solutions that travel with the same speed as the source. In such a case we can assume that the source term S is also a function of $\zeta = x - Mt$ (in other words $v_d = M$, where v_d is the debris velocity).
Then, taking $\beta = 0$, eqns.(10), (11), (12) and (13) can be transformed to,

$$M\frac{\partial v_y}{\partial \zeta} = -\sin(\theta)\frac{\partial b_y}{\partial \zeta} - S(\cos(\theta) + b_z) \tag{38}$$

$$M\frac{\partial v_z}{\partial \zeta} = -\sin(\theta)\frac{\partial b_z}{\partial \zeta} + Sb_y \tag{39}$$

$$-M\frac{\partial b_y}{\partial \zeta} = -\frac{\partial}{\partial \zeta}(v_x b_y - v_y \sin(\theta)) + \frac{\partial}{\partial \zeta}(\frac{1}{n}\sin(\theta)\frac{\partial b_z}{\partial \zeta}) + \frac{\partial}{\partial \zeta}\left(\frac{Sb_y}{n}\right) \tag{40}$$

$$-M\frac{\partial b_z}{\partial \zeta} = \frac{\partial}{\partial \zeta}(v_z \sin(\theta) - v_x(\cos(\theta) + b_z)) - \frac{\partial}{\partial \zeta}(\frac{1}{n}\sin(\theta)\frac{\partial b_y}{\partial \zeta}) + \frac{\partial}{\partial \zeta}\left(\frac{S(\cos(\theta) + b_z}{n}\right) \tag{41}$$

Equations (40) and (41 can be integrated once to get,

$$\sin(\theta)\frac{\partial b_z}{\partial \zeta} + Mb_y + nv_y \sin(\theta) - S)b_y = 0 \tag{42}$$

$$\sin(\theta)\frac{\partial b_y}{\partial \zeta} - Mb_z - nv_z \sin(\theta) + nv_x \cos(\theta) - S(\cos(\theta) + b_z) = 0 \tag{43}$$

where we have used eqn.(24). The expression of n is given by eqn.(32).

We have numerically solved the coupled equations (38), (39), (42) and (43) with a source term of the form $S = A_0 e^{-\zeta^2/\Delta^2}$ where A_0 and Δ are constants. A plot of a typical pinned soliton at $M = 0.0185$ in the presence of a weak source term, with $A_0 = 1.5 \times 10^{-6}$ and

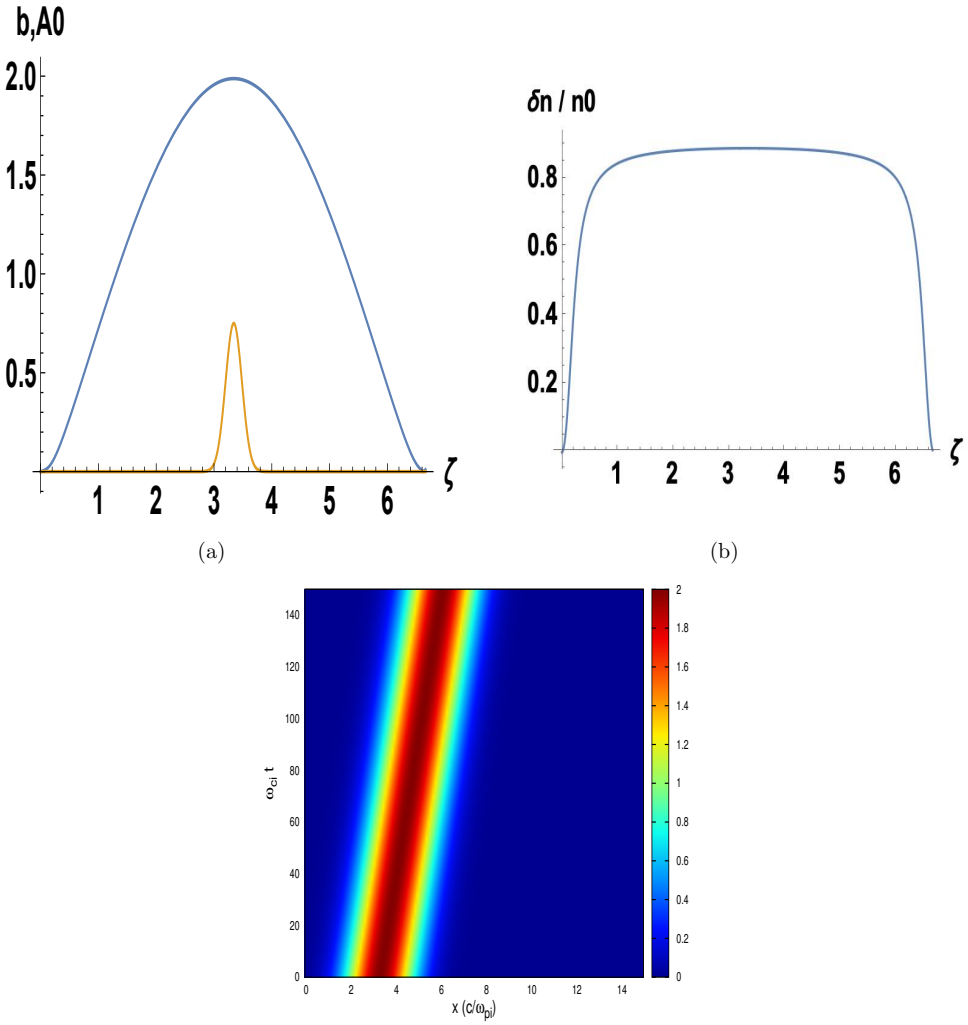

(a) (b)

(c)

FIG. 7: (a) Pinned Ion inertial wave soliton with $M = 0.0185$, $\beta = 0$, $\theta = 1^0$, $A0 = 1.5 \times 10^{-6}$ and $\Delta = 0.2$. The source term (orange) is multiplied by 4×10^4 to make it visible on plot. (b) The density perturbation corresponding to the magnetic field perturbations of (a). (c) Time evolution of this soliton shown in terms of b_z. This is obtained by simultaneously solving eqns. (8-13), with the initial condition taken from the solution of eqns. (42, 43) and eqn. (32)

$\Delta = 0.2$ is shown in Fig.7a. The amplitude of the source term is multiplied by a factor of 5×10^4 to display it on the same plot. Fig.7b shows the corresponding perturbed density profile of the soliton which can be seen to be quite large and to span a large spatial extent. The density perturbations also constitute a significant fraction of the background density value and can therefore be above the level of natural density fluctuations in the region. In Fig.7c we show the time evolution plot of this soliton. The nature of the pinned soliton is quite similar to the one that was obtained with the reduced model equation, namely, the fKdV equation (15) with $\beta = 0$. This can be understood from the linear dispersion relation given by eq.(14). Putting $\beta = 0$ and taking the limit of small θ it can be easily shown that the linear ion inertial wave solution takes the form,

$$M_1 = \frac{\omega}{kV_A} = 1 + k^2\delta^2\theta^2$$

which has the same form as the dispersion relation for an ion acoustic wave. The dispersion in this case is provided by the ion inertial contribution $k^2\delta^2$ instead of the thermal pressure term. Thus in the small propagation angle limit, the region where these small M solitons exist, the fKdV equation provides a good model description.

V. DISCUSSION AND CONCLUSIONS

To summarize, we have generalized our electrostatic formalism of debris generated solitons[12] to electromagnetic and investigated the existence and nature of electromagnetic solitons that can be excited by an external moving current source term. We have done this in the framework of an inertial magneto-hydrodynamic model. Our numerical and analytic solutions in special limits, reveal a rich variety of soliton solutions that can arise from the nonlinear evolution of Alfvén waves, magneto-sonic waves or the low frequency inertial ion waves. These can have a wide variety of applications in situations where a current source traverses through a magnetised plasma. Our particular motivation for studying these nonlinear structures is to exploit them for the identification and tracking of small sized (sub-cm) orbital space debris objects that are difficult to track optically. In our earlier study[12], carried out for electrostatic ion acoustic waves, it was suggested that detection of precursor ion acoustic solitons emitted by the charged debris object, could provide an indirect means of tracking the trajectory of orbital debris objects. Our present work extends

this concept in two directions. Firstly, we propose that another class of solitons discussed by us earlier[12], called pinned solitons, which can also be excited by the moving source, may provide a more direct means of tracking the debris objects as they travel with the same speed as the object and remain pinned to the object. Secondly, as electromagnetic nonlinear structures, their spatial widths are typically of the order of a few ion skin depths, that are much larger than the Debye length envelopes provided by the electrostatic solitons. Thus these electromagnetic solitons would be easier to detect by radar scattering techniques. As a historical aside, and to put our present work in the broader context of previous research and other approaches, it is worth mentioning that the topic of interaction of a fast moving body with the ionosphere and lower atmosphere had received considerable attention in the late fifties[36,37] and early sixties[38,39] in the context of determining satellite drag. The development of wave structures like the bow wave in front of the satellite and a wake structure trailing the satellite were discussed[39]. The bow wave resulting from an accumulation of particles due to reflection off the satellite surface is always present and surrounds the front portion of the traveling body. Such a density build up has a strong similarity with the "pinned" soliton discussed by us. However, it should be noted that the bow wave structures discussed in these past works had been obtained from a linear analysis of the plasma equations as distinct from our present nonlinear analysis. Our electromagnetic nonlinear structures in the form of pinned solitons are therefore quite distinct from the linear bow wave solutions. They are part of a larger class of nonlinear solutions that include precursor solitons, shock structures and oscillatory nonlinear wake fields.

We now discuss our results in the context of the LEO region. The typical plasma parameters[21,22] in this region at an altitude of around 600 kms are, $n_{0e} \sim n_{0i} \sim 10^6 cm^{-3}; T_e \sim 2200K; T_i \sim 600K; \mu = \frac{m_i}{m_p} = \frac{1}{16}$ where $m_i = 16m_p$ is the mass of the ion and m_p is the mass of the proton. The ion species is predominantly O^+ in this region. n_{0e}, n_{0i} denote the number densities of the electrons and ions respectively while T_e and T_i are the electron and ion temperatures. The electron plasma skin length for these parameters is about 5.3 m whereas the ion skin depth is around 1 km.

The typical magnetic field in this region is of the order of 0.3 to 0.5 Gauss. The Alfven velocity is then in the range of $160km/s$ to $320km/s$. The debris velocity in this region is about $8km/s$. Hence in order for the debris to latch on to a pinned soliton traveling at its own velocity we need to consider solitons that have a Mach number that is less than ~ 0.05.

Also the plasma β in this region is of the order of 10^{-4} and hence has a negligible effect on the dynamics. Thus the pinned soliton solutions that are relevant for this region are the low Mach number ion inertial wave solitons, a typical example of which is shown in Fig.7. It should be mentioned that we have not taken collisional effects into account which could lead to damping or other structural changes of the soliton. This could be important for precursor solitons which once created detach themselves from the driving source and propagate freely in the plasma ahead of the source. These solitons would then suffer exponential damping in their amplitude as has been shown experimentally for dust acoustic precursor solitons by Jaiswal *et al.*[13]. The effect has also been studied theoretically using numerical solutions of the fKdV equation modified to include damping by Truitt and Hartzell[18]. However, for pinned solitons, the subject of our present analysis, collisions/dissipation effects do not have any significant effect as the solitons are continuously being fed energy from the driving source. This has also been pointed out by Truitt and Hartzell[18].

Although the primary focus of this article is to generalize our electrostatic formalism for the forced KdV solitons to the electromagnetic regime, we note that there are means of detecting such soliton structures. In addition, a major thrust of the Intelligence Advanced Research Project Activity (IARPA)[40] initiative is to develop other means for detection, especially those with poor signal to noise ratios. While a detailed discussion of detection techniques is beyond the scope of this article, we note that nonlinear coherent structures consisting of large amplitude density fluctuations or magnetic field perturbations naturally exist in the ionosphere from nonlinear saturation of instabilities of various plasma modes in the system. A few examples of such structures are ion or electron acoustic solitons and double layers found in the satellite measurements of broadband electrostatic noise (BEN) (see review by Lakhina *et. al.*[41] and references therein), equatorial plasma bubbles (EPBs) found in the F region (see review by Bhattacharyya[42] and references therein) and magnetosonic solitons found in the magnetopause boundary layer[43]. These nonlinear plasma irregularities that span a wide range of space and time scales are routinely measured using a variety of instruments such as digisondes, coherent and incoherent scatter radars, in-situ space probes, and airglow photometers[41]. Since the debris induced solitons are large amplitude fluctuations and have scale sizes that fall in the range of the irregularities like the Equatorial Spread F (ESF) or EPBs, they should be detectable by these methods. A majority of the

detection techniques rely on the scattering of a radio wave off the plasma fluctuation structure. For example, the incoherent scattering of a transmitted radar wave propagating in the ionosphere normally occurs due to the ambient thermal fluctuations giving rise to a weak scattered signal. The presence of a structure like a soliton or a bubble, that has a large density perturbation, can lead to a strong coherent back scatter signal that can show up against the background of the weak incoherent scatter data as a distinct signature of the soliton presence. There can also be noticeable changes in the incoherent spectra. For example, the presence of a low frequency soliton (e.g. ion acoustic or magnetosonic soliton) can give rise to spectrally uniform enhancement in the incoherent ion-line[44]. Such observations have been reported by the EISCAT Svalbard Radar (ESR) and could serve as a useful diagnostic for detecting the presence of debris induced magneto-sonic solitons[45]. The scattering data can be generated using either ground based radar facilities or by satellite based top sounders[46]. A related technique is to observe the scintillations produced by the scattering of the top side injected radio wave as it passes through the nonlinear structure[42]. Such measurements have yielded useful information about the structure and dynamics of EPBs[42] and can be adapted for debris induced solitons in the LEO region. It should be mentioned here that large sized (> 10 cm) debris are routinely tracked and catalogued using a combination of ground based and space based measurements[8,47,48]. However, radar observations of small sized debris still pose a challenge and are normally carried out in the 'staring' mode of the radar that measures the debris flux passing through the beam width. This provides important statistical information regarding the distribution of small sized debris in a particular environment and helps in the construction of debris population models[49,50]. Present technological advances are rapidly enhancing the potential capabilities of ground based radars and also developing space based radar scattering facilities using micro-satellites[51] and CUBE-SATS[52]. Some of these planned future devices, such as EISCAT-3D aim to directly track sub-cm debris objects[53–55] in the coherent scattering mode. These radars would also be engaged in doing incoherent scattering experiments and could therefore additionally provide information on the soliton structures induced by the debris.

To conclude, in our present work we have provided a conceptual extension of our earlier work on electrostatic pinned solitons to electromagnetic ones. There are inherent advantages to using electromagnetic solitons versus electrostatic ones to detect orbital debris, namely,

their scale sizes are larger and they are free of Landau damping effects which would suggest they are longer lived. Their scale sizes and amplitudes fall in the range of many naturally occurring plasma irregularities and hence they should be detectable using present day ground based and satellite based radar scattering techniques. As in the case of electrostatic solitons the detection and tracking of these electromagnetic solitons could prove useful in the detection of small sized orbital debris objects. A practical scheme to exploit this concept needs to be further developed keeping in mind the presently existing debris detection capabilities. It is hoped that our results will stimulate such development activities and lead to engineering feasibility studies. This study is particularly relevant and timely now because orbital debris related hazards are beginning to threaten our on-demand access to space, and in response IARPA, U.S.A., has initiated a debris-generated soliton tracking and detection program[40]. Use of radars to detect solitons is one of the objectives of this program.

Appendix A: Derivation of the fKdV equation

We briefly outline here the derivation of the fKdV equation (15), by applying a reduction perturbation analysis to the set of equations (8 - 13). We adopt the following expansion for the physical quantities, $f = \{n, v_x, v_y, v_z, B_x, B_y, B_z\}$,

$$f = f_0 + \epsilon f_1 + \epsilon^2 f_2 + \epsilon^3 f_3 + O(\epsilon^4)$$

where $f_0 = \{1, 0, 0, 0, sin(\theta), 0, cos(\theta)\}$ and $f_j = \{n_j, v_{xj}, v_{yj}, v_{zj}, 0, b_{yj}, b_{zj}\}$ with $j = 1, 2, 3, ...$ We also take

$$S = \epsilon^2 S_2$$

and define the following set of stretched variables,

$$\xi = \epsilon^{1/2}(x - Mt) \;\; ; \;\; \tau = \epsilon^{3/2} t$$

where M is the normalized wave velocity. Expressing the differential operators in terms of these stretched variable gives us,

$$\frac{\partial}{\partial x} = \epsilon^{1/2}\frac{\partial}{\partial \xi} \;\; ; \;\; \frac{\partial}{\partial t} = -M\epsilon^{1/2}\frac{\partial}{\partial \xi} + \epsilon^{3/2}\frac{\partial}{\partial \tau} \; ; \; \frac{\partial^2}{\partial x^2} = \epsilon\frac{\partial^2}{\partial \xi^2}$$

Using the above expansions in the equations (8-13) and following the standard procedure of collecting terms of the same order of ϵ, we can obtain the following from each of the equations,

$$\epsilon^{3/2}: \quad -M\frac{\partial n_1}{\partial \xi} + \frac{\partial v_{x1}}{\partial \xi} = 0 \tag{A1}$$

$$\epsilon^{5/2}: \quad -M\frac{\partial n_2}{\partial \xi} + \frac{\partial n_1}{\partial \tau} + \frac{\partial (n_1 v_{x1})}{\partial \xi} + \frac{\partial v_{x2}}{\partial \xi} = 0 \tag{A2}$$

$$\epsilon^{3/2}: \quad -M\frac{\partial v_{x1}}{\partial \xi} + cos\theta\frac{\partial b_{z1}}{\partial \xi} + \beta\frac{\partial n_1}{\partial \xi} = 0 \tag{A3}$$

$$\epsilon^{5/2}: \quad -M\frac{\partial v_{x2}}{\partial \xi} + \frac{\partial v_{x1}}{\partial \tau} + v_{x1}\frac{\partial v_{x1}}{\partial \xi} + cos\theta\frac{\partial b_{z2}}{\partial \xi} - Mn_1\frac{\partial v_{x1}}{\partial \xi} + b_{z1}\frac{\partial b_{z1}}{\partial \xi} + \beta\frac{\partial n_2}{\partial \xi} = 0 \tag{A4}$$

$$\epsilon^{3/2}: \quad -M\frac{\partial v_{y1}}{\partial \xi} - sin\theta\frac{\partial b_{y1}}{\partial \xi} = 0 \tag{A5}$$

$$\epsilon^{5/2}: \quad -M\frac{\partial v_{y2}}{\partial \xi} + \frac{\partial v_{y1}}{\partial \tau} + v_{x1}\frac{\partial v_{y1}}{\partial \xi} - sin\theta\frac{\partial b_{y2}}{\partial \xi} + sin\theta n_1\frac{\partial b_{y1}}{\partial \xi} = 0 \tag{A6}$$

$$\epsilon^{3/2}: \quad -M\frac{\partial v_{z1}}{\partial \xi} - sin\theta\frac{\partial b_{z1}}{\partial \xi} = 0 \tag{A7}$$

$$\epsilon^{5/2}: \quad -M\frac{\partial v_{z2}}{\partial \xi} + \frac{\partial v_{z1}}{\partial \tau} + v_{x1}\frac{\partial v_{z1}}{\partial \xi} - sin\theta\frac{\partial b_{z2}}{\partial \xi} - Mn_1\frac{\partial v_{z1}}{\partial \xi} = 0 \tag{A8}$$

$$\epsilon^{3/2}: \quad -M\frac{\partial b_{y1}}{\partial \xi} - sin\theta\frac{\partial v_{y1}}{\partial \xi}1 = 0 \tag{A9}$$

$$\epsilon^{5/2}: \quad -M\frac{\partial b_{y2}}{\partial \xi} + \frac{\partial b_{y1}}{\partial \tau} - sin\theta\frac{\partial v_{y2}}{\partial \xi} + \frac{\partial (v_{x1}b_{y1})}{\partial \xi} \tag{A10}$$

$$\epsilon^{3/2}: \quad -M\frac{\partial b_{z1}}{\partial \xi} - sin\theta\frac{\partial v_{z1}}{\partial \xi} + cos\theta\frac{\partial v_{x1}}{\partial \xi} = 0 \tag{A11}$$

$$\epsilon^{5/2}: \quad -M\frac{\partial b_{z2}}{\partial \xi} + \frac{\partial b_{z1}}{\partial \tau} - sin\theta\frac{\partial v_{z2}}{\partial \xi} + \frac{\partial (v_{x1}b_{z1})}{\partial \xi} + cos(\theta)\frac{\partial v_{x2}}{\partial \xi} - M\frac{\partial^2 v_{y1}}{\partial \xi^2} - cos(\theta)\frac{\partial S_2}{\partial \xi} = 0 \tag{A12}$$

Integrating equations (A1),(A3), (A7) and (A11) we get,

$$\begin{aligned} -Mn_1 + v_{x1} &= 0 \\ -Mv_{x1} + cos\theta b_{z1} + \beta n_1 &= 0 \\ -Mv_{z1} - sin\theta b_{z1} &= 0 \\ -MB_{z1} - sin\theta v_{z1} + cos\theta v_{x1} &= 0 \end{aligned} \tag{A13}$$

From eqns. (A13) we get a dispersion relation,

$$M^2(M^2-1) + \beta(sin^2\theta - M^2) = 0 \tag{A14}$$

This is the dispersion relation for magneto-sonic waves. Next we consider eqns. (A2), (A4), (A8), (A12) and rewrite them as follows,

$$\begin{aligned} -M\frac{\partial n_2}{\partial \xi} + \frac{\partial v_{x2}}{\partial \xi} &= -T_1 \\ \beta\frac{\partial n_2}{\partial \xi} - M\frac{\partial v_{x2}}{\partial \xi} + cos\theta\frac{\partial b_{z2}}{\partial \xi} &= -T_2 \\ -M\frac{\partial v_{z2}}{\partial \xi} - sin\theta\frac{\partial b_{z2}}{\partial \xi} &= -T_3 \\ -M\frac{\partial b_{z2}}{\partial \xi} - sin\theta\frac{\partial v_{z2}}{\partial \xi} + cos(\theta)\frac{\partial v_{x2}}{\partial \xi} &= -T_4 \end{aligned} \tag{A15}$$

where,

$$\begin{aligned} T_1 &= \frac{\partial n_1}{\partial \tau} + v_{x1}\frac{\partial n_1}{\partial \xi} + n_1\frac{\partial v_{x1}}{\partial \xi} \\ T_2 &= \frac{\partial v_{x1}}{\partial \tau} + v_{x1}\frac{\partial v_{x1}}{\partial \xi} - Mn_1\frac{\partial v_{x1}}{\partial \xi} + b_{z1}\frac{\partial b_{z1}}{\partial \xi} \\ T_3 &= \frac{\partial v_{z1}}{\partial \tau} + v_{x1}\frac{\partial v_{z1}}{\partial \xi} - Mn_1\frac{\partial v_{z1}}{\partial \xi} \\ T_4 &= \frac{\partial b_{z1}}{\partial \tau} + \frac{\partial (v_{x1}b_{z1})}{\partial \xi} - M\frac{\partial^2 v_{y1}}{\partial \xi^2} - cos(\theta)\frac{\partial S_2}{\partial \xi} \end{aligned} \tag{A16}$$

The set of equations (A15) can be expressed in the form,

$$\begin{pmatrix} -M & 1 & 0 & 0 \\ \beta & -M & 0 & cos\theta \\ 0 & 0 & -M & -sin\theta \\ 0 & cos\theta & -sin\theta & -M \end{pmatrix} \begin{pmatrix} \partial n_2/\partial \xi \\ \partial v_{x2}/\partial \xi \\ \partial v_{z2}/\partial \xi \\ \partial b_{z2}/\partial \xi \end{pmatrix} = \begin{pmatrix} -T_1 \\ -T_2 \\ -T_3 \\ -T_4 \end{pmatrix} \tag{A17}$$

To obtain the solvability condition for the set of equations (A17) one can start by constructing an extended matrix,

$$E = \begin{pmatrix} -M & 1 & 0 & 0 & | & T_1 \\ \beta & -M & 0 & cos\theta & | & T_2 \\ 0 & 0 & -M & -sin\theta & | & T_3 \\ 0 & cos\theta & -sin\theta & -M & | & T_4 \end{pmatrix} \tag{A18}$$

which by a few simple matrix operations, (A17) can be converted to the following form,

$$\tilde{\tilde{E}}_2 = \begin{pmatrix} 1 & -1/M & 0 & 0 & | & -T_1/M \\ 0 & 1 & 0 & -\frac{cos\theta/M}{(1-\beta/M^2)} & | & -\frac{(\beta T_1/M^2+T_2/M)}{(1-\beta/M^2)} \\ 0 & 0 & 1 & sin\theta/M & | & -T_3/M \\ 0 & 0 & 0 & D_1 & | & D_2 \end{pmatrix} \tag{A19}$$

where $D_1 = M^2(1+\beta) - M^4 - \beta sin^2\theta$ and $D_2 = T_1 \times M \times cos\theta \times \beta + T_2 \times cos\theta \times M^2 + T_3 \times sin\theta \times (\beta - M^2) + T_4 \times M \times (M^2 - \beta)$. For (A17) to have solutions the entries in the bottom row of $\tilde{\tilde{E}}_2$ should all be zero. Now $D_1 = 0$ by virtue of the dispersion relation (A14). So the solvability condition is $D_2 = 0$ Substituting for T_1, T_2, T_3 and T_4 in D_2 we get,

$$\begin{aligned} &\beta cos\theta \left[\frac{\partial n_1}{\partial \tau} + v_{x1}\frac{\partial n_1}{\partial \xi} + n_1\frac{\partial v_{x1}}{\partial \xi}\right] + M^2 cos\theta \left[\frac{\partial v_{x1}}{\partial \tau} + v_{x1}\frac{\partial v_{x1}}{\partial \xi} - Mn_1\frac{\partial v_{x1}}{\partial \xi} + b_{z1}\frac{\partial b_{z1}}{\partial \xi}\right] \\ &+ (\beta - M^2) sin\theta \left[\frac{\partial v_{z1}}{\partial \tau} + v_{x1}\frac{\partial v_{z1}}{\partial \xi} - Mn_1\frac{\partial v_{z1}}{\partial \xi}\right] \\ &+ M(M^2 - \beta)\left[\frac{\partial b_{z1}}{\partial \tau} + \frac{\partial (v_{x1}b_{z1})}{\partial \xi} - M\frac{\partial^2 v_{y1}}{\partial \xi^2} - cos(\theta)\frac{\partial S_2}{\partial \xi}\right] = 0 \end{aligned} \tag{A20}$$

From (A9) and (A13) we can get,

$$n_1 = v_{x1}\ ;\ b_{z1} = \frac{M-\beta}{cos\theta}v_{x1}\ ;\ v_{z1} = -tan\theta\frac{M-\beta}{M}v_{x1}\ ;\ v_{y1} = \frac{Msin^2\theta}{M^2 - sin^2\theta}\frac{(M-\beta)}{Mcos\theta}\frac{\partial v_{x1}}{\partial \xi}$$

Using the above relations we can express eqn. (A20) in terms of a single variable, namely, b_{z1}. The final equation is,

$$a_1\frac{\partial b_{z1}}{\partial \tau} + a_2 b_{z1}\frac{\partial b_{z1}}{\partial \xi} + a_3\frac{\partial^3 b_{z1}}{\partial \xi^3} = cos(\theta)\frac{\partial S_2}{\partial \xi} \tag{A21}$$

where,

$$a_1 = (\beta + M^2)cos(\theta) - \frac{(\beta - M^2)((M-\beta)}{M}sin(\theta)tan(\theta) + \frac{M(M^2-\beta)(M-\beta)}{cos(\theta)}$$

$$a_2 = 2\frac{\beta}{M-\beta}cos^2(\theta) + \left(1 - M + \frac{(M-\beta)^2}{cos^2(\theta)}\right)\frac{M^2}{M-\beta}cos^2(\theta) + \frac{(M^2-\beta)(1-M)}{M}sin^2(\theta) + 2M(M^2-\beta)$$

$$a_3 = -\frac{(M^2-\beta)(M-\beta)M^2 tan(\theta)sin(\theta)}{(M^2 - sin^2(\theta))}$$

Acknowledgement

A.S. acknowledges AOARD for their research grant FA2386-18-1-4022 and is grateful to the Indian National Science Academy for the Honorary Scientist position. Work at NRL is supported by NRL Base Funds.

DATA AVAILABILITY

The data that support the findings of this study are available from the corresponding author upon reasonable request.

REFERENCES

[1] "Low earth orbit visualization," `https://platform.leolabs.space/visualization`.

[2] L. Perek, Space Debris **2**, 123 (2000).

[3] A. Horstmann, C. Kebschull, S. Müller, E. Gamper, S. Hesselbach, K. Soggeberg, M. K. Ben Larbi, M. Becker, J. Lorenz, C. Wiedemann, and E. Stoll, Aerospace **5** (2018), 10.3390/aerospace5020037.

[4] A. Murtaza, S. J. H. Pirzada, T. Xu, and L. Jianwei, IEEE Access **8**, 61000 (2020).

[5] E. Christiansen, J. Hyde, and R. Bernhard, Advances in Space Research **34**, 1097 (2004), space Debris.

[6] J.-C. Liou, 28th International Symposium on Space Technology and Science, Okinawa, Japan, June 5-12 (2011).

[7] W. Flury, A. Massart, T. Schildknecht, U. Hugentobler, J. Kuusela, and Z. Sodnik, ESA bulletin **104**, 92–100 (2000).

[8] D. Mehrholz, L. Leushacke, W. Flury, R. Jehn, H. Klinkrad, and M. Landgraf, ESA bulletin **109**, 128 (2002).

[9] J. Goree, Plasma Sources, Science and Technology **3**, 400 (1994).

[10] A. Juhasz and M. Horanyi, Journal of Geophysical Research **102**, 7237 (1997).

[11]W. J. Miloch, H. L. Pécseli, and J. Trulsen, Nonlinear Processes in Geophysics **14**, 575 (2007).

[12]A. Sen, S. Tiwari, S. Mishra, and P. Kaw, Advances in Space Research **56**, 429 (2015).

[13]S. Jaiswal, P. Bandyopadhyay, and A. Sen, Phys. Rev. E **93**, 041201(R) (2016).

[14]S. K. Tiwari and A. Sen, Physics of Plasmas **23**, 022301 (2016).

[15]S. K. Tiwari and A. Sen, Physics of Plasmas **23**, 100705 (2016), https://doi.org/10.1063/1.4964908.

[16]G. Arora, P. Bandyopadhyay, M. G. Hariprasad, and A. Sen, Physics of Plasmas **26**, 093701 (2019), https://doi.org/10.1063/1.5115313.

[17]A. S. Truitt and C. M. Hartzell, Journal of Spacecraft and Rockets **57**, 876 (2020), https://doi.org/10.2514/1.A34652.

[18]A. S. Truitt and C. M. Hartzell, Journal of Spacecraft and Rockets **57**, 975 (2020), https://doi.org/10.2514/1.A34674.

[19]A. S. Truitt and C. M. Hartzell, Journal of Spacecraft and Rockets **58**, 848 (2021), https://doi.org/10.2514/1.A34805.

[20]G. Arora, P. Bandyopadhyay, M. G. Hariprasad, and A. Sen, Phys. Rev. E **103**, 013201 (2021).

[21]A. Gurevich, Nonlinear phenomena in the ionosphere, Vol. 10 (Springer Science & Business Media, 1978).

[22]M. C. Kelley, The Earth's ionosphere: Plasma physics and electrodynamics (Academic press, 2009).

[23]V. V. Gavrishchaka, S. B. Ganguli, and G. I. Ganguli, Phys. Rev. Lett. **80**, 728 (1998).

[24]Y. A. Berezin and V. Karpman, Soviet Physics JETP **19**, 1265 (1964).

[25]R. Fitzpatrick, Plasma physics: an introduction (Crc Press, 2014).

[26]A. Kumar and A. Sen, New Journal of Physics **22**, 073057 (2020).

[27]A. Sen, S. Yadav, G. Ganguli, and C. Crabtree, 2019 International Conference on Electromagnetics in Advanced Applications (ICEAA), Granada, Spain, 9-13 September 2019 , 156 (2019).

[28]A. Sen, A. Kumar, S. Yadav, G. Ganguli, and C. Crabtree, 2021 International Conference on Electromagnetics in Advanced Applications (ICEAA), Honolulu, Hawaii, U.S.A. , 09 - 13 August 2021 , 32 (2021).

[29]T. R. Akylas, J. Fluid Mech. **141**, 455 (1984).

[30]R. Camassa and T. Wu, Physica D: Nonlinear Phenomena **51**, 295 (1991).

[31]H. Lewy, K. Friedrichs, and R. Courant, Mathematische annalen **100**, 32 (1928).

[32]K. Stasiewicz, Journal of Geophysical Research: Space Physics **110** (2005).

[33]M. Gedalin, Physics of Plasmas **5**, 127 (1998).

[34]J. H. Adlam and J. E. Allen, The Philosophical Magazine: A Journal of Theoretical Experimental and Applied Physics **3**, 448 (1958), https://doi.org/10.1080/14786435808244566.

[35]J. H. Adlam and J. E. Allen, Proceedings of the Physical Society **75**, 640 (1960).

[36]R. Jastrow and C. A. Pearse, Journal of Geophysical Research (1896-1977) **62**, 413 (1957), https://agupubs.onlinelibrary.wiley.com/doi/pdf/10.1029/JZ062i003p00413.

[37]L. Kraus and K. M. Watson, Physics of Fluids **1**, 480 (1958).

[38]K. P. Chopra, Rev. Mod. Phys. **33**, 153 (1961).

[39]Y. L. Al'pert, A. V. Gurevich, and L. P. Pitaevskiĭ, Soviet Physics Uspekhi **6**, 13 (1963).

[40]`https://govtribe.com/opportunity/federal-contract-opportunity/orbital-debris-detection-and-tracking-request-for-information-iarparfi2204` (2022).

[41]G. S. Lakhina, S. Singh, R. Rubia, and S. Devanandhan, Plasma **4**, 681 (2021).

[42]A. Bhattacharyya, Atmosphere **13** (2022), 10.3390/atmos13101637.

[43]K. Stasiewicz, P. K. Shukla, G. Gustafsson, S. Buchert, B. Lavraud, B. Thidé, and Z. Klos, Phys. Rev. Lett. **90**, 085002 (2003).

[44]J. Ekeberg, G. Wannberg, L. Eliasson, and K. Stasiewicz, Annales Geophysicae **28**, 1299 (2010).

[45]J. Ekeberg, G. Wannberg, L. Eliasson, and I. Häggström, Earth, Planets and Space **64**, 605 (2012).

[46]W. Calvert and J. Warnock, Proceedings of the IEEE **57**, 1019 (1969).

[47]M. Nicolls, in Advanced Maui Optical and Space Surveillance Technologies Conference (2015) p. 87.

[48]J. Wang, X. Yue, F. Ding, B. Ning, L. Jin, C. Ke, N. Zhang, Y. Wang, H. Yin, M. Li, and Y. Cai, Radio Science **57**, e2022RS007472 (2022), https://agupubs.onlinelibrary.wiley.com/doi/pdf/10.1029/2022RS007472.

[49]E. Stansbery, D. Kessler, T. Tracy, M. Matney, and J. Stanley, Advances in Space Research **16**, 5 (1995).

[50]Y.-L. Xu, T. Kennedy, and E. Stansbery, First International Orbital Debris Conference

(2019) (2019).

[51]A. Houpert, Acta Astronautica **44**, 313 (1999), pacific RIM: A Rapidly Expanding Space Market.

[52]A. Persico, P. Kirkland, C. Clemente, J. Soraghan, and M. Vasile, IEEE Transactions on Aerospace and Electronic Systems **55**, 476 (2019).

[53]J. Vierinen, J. Markkanen, H. Krag, J. Siminski, and A. Mancas, in ESA Space Debris Office proceedings, T. Flohrer and F. Schmitz (eds.), Vol. 7(1) (2017).

[54]J. Vierinen, T. Crydeland, D. Kastinen, C. Kebschull, J. Kero, and H. Krag, in 2018 2nd URSI Atlantic Radio Science Meeting (AT-RASC) (2018) pp. 1–1.

[55]D. Kastinen, T. Tveito, J. Vierinen, and M. Granvik, Annales Geophysicae **38**, 861 (2020).

PLEASE CITE THIS ARTICLE AS DOI: 10.1063/5.0099201

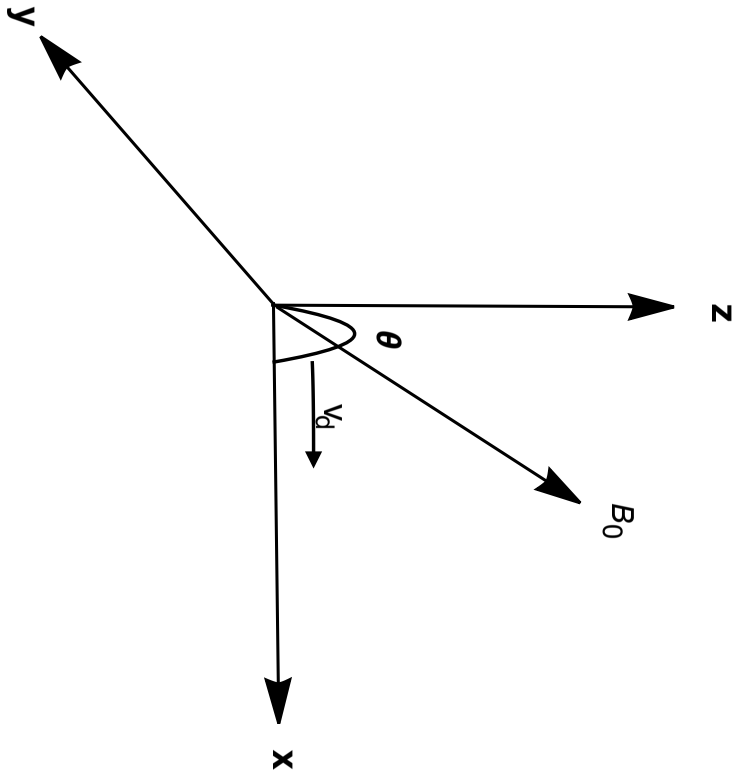

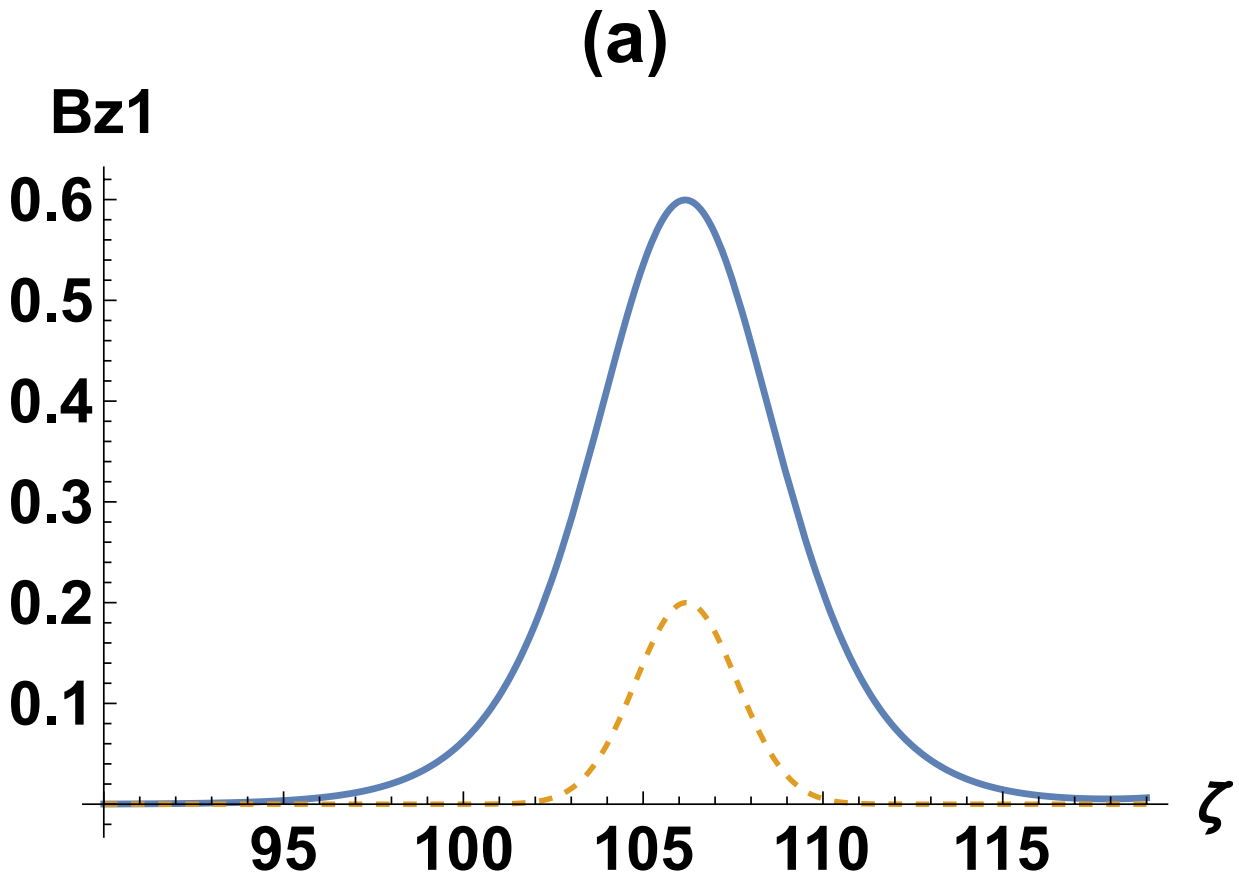

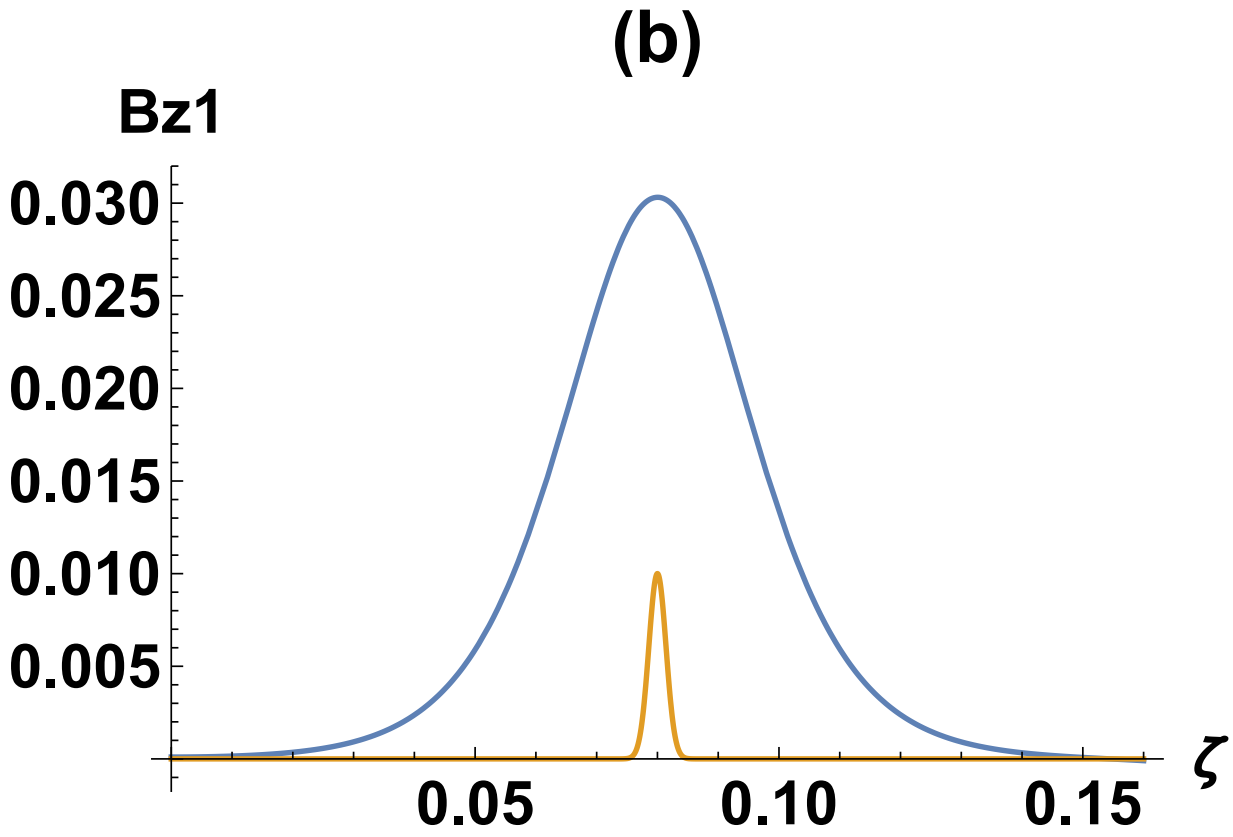

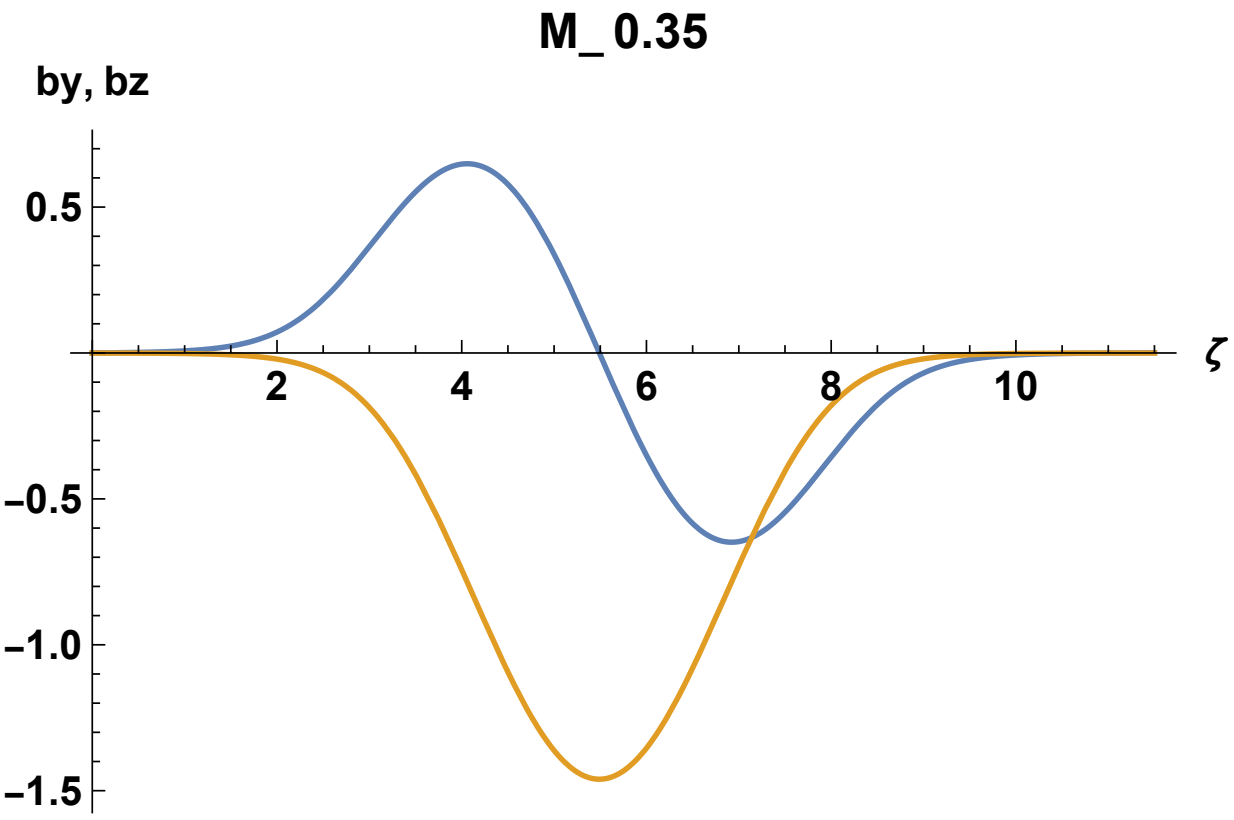

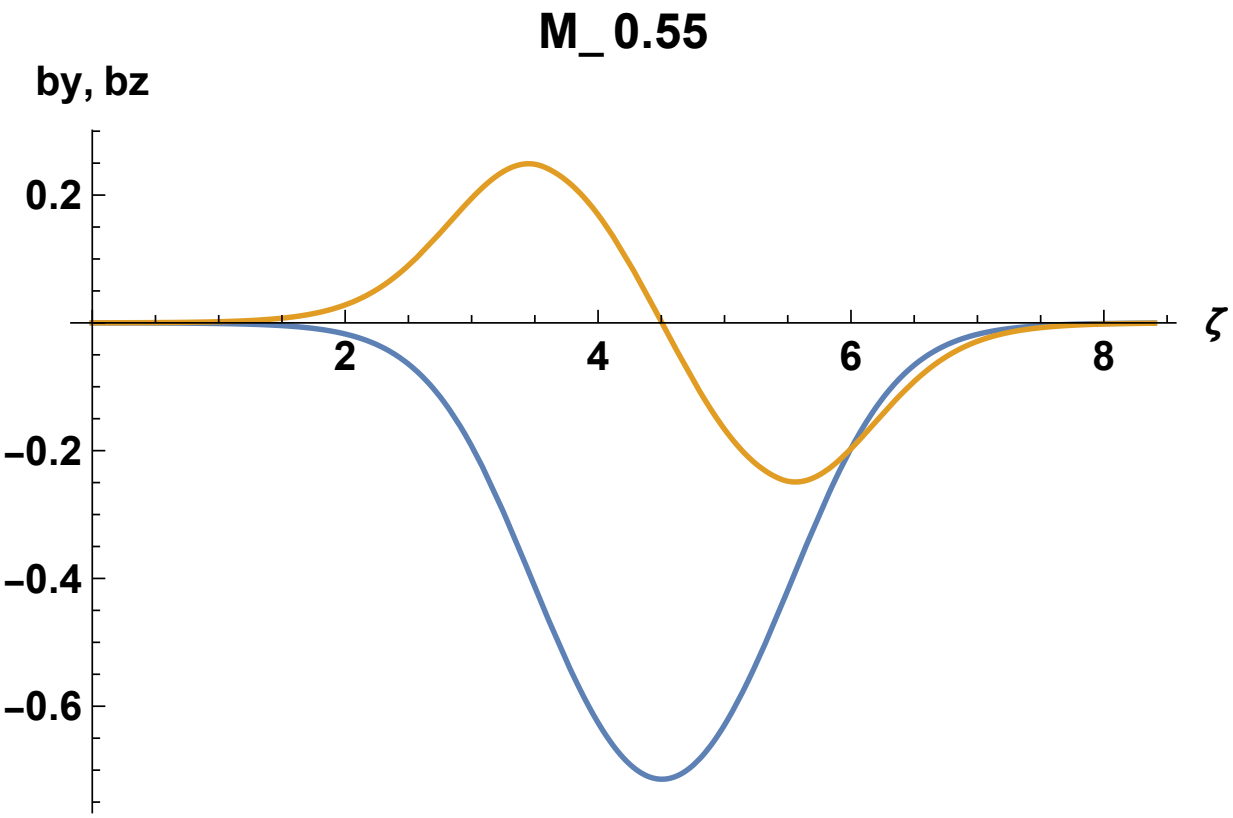

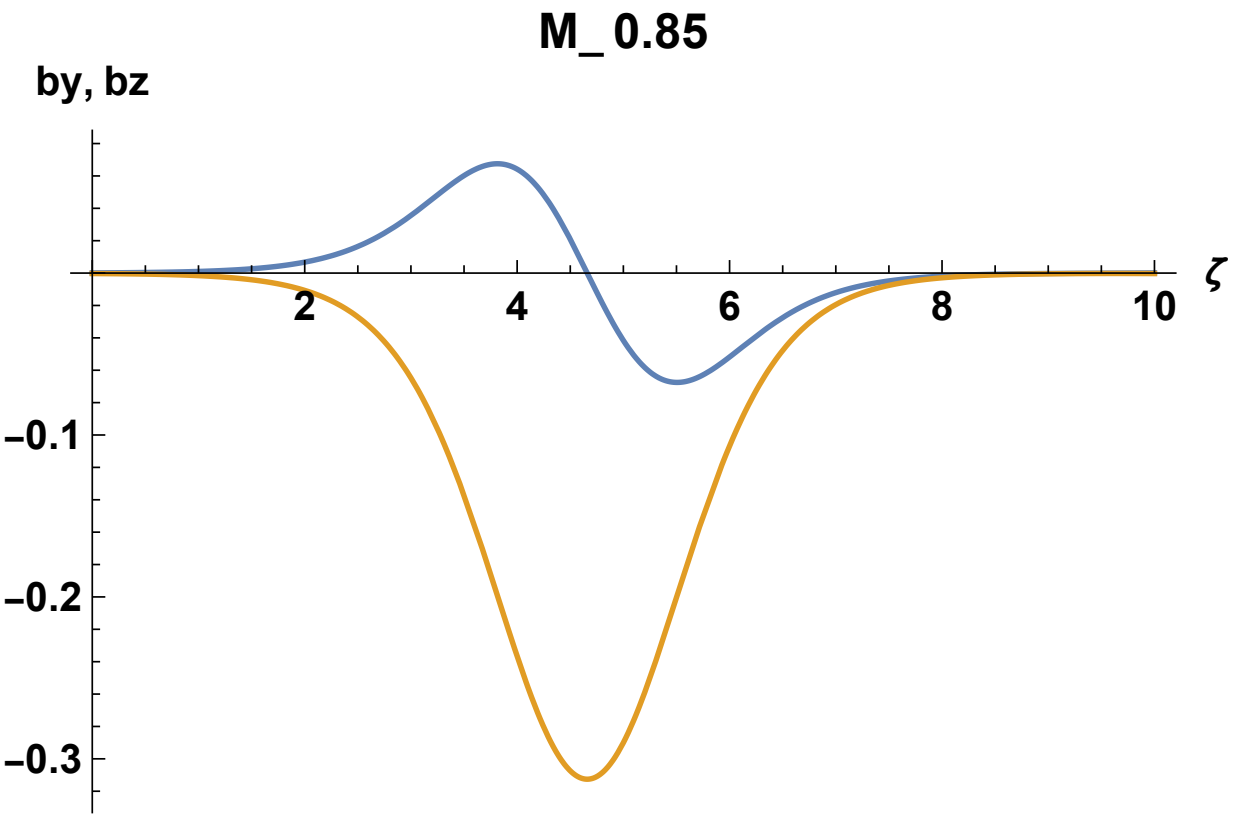

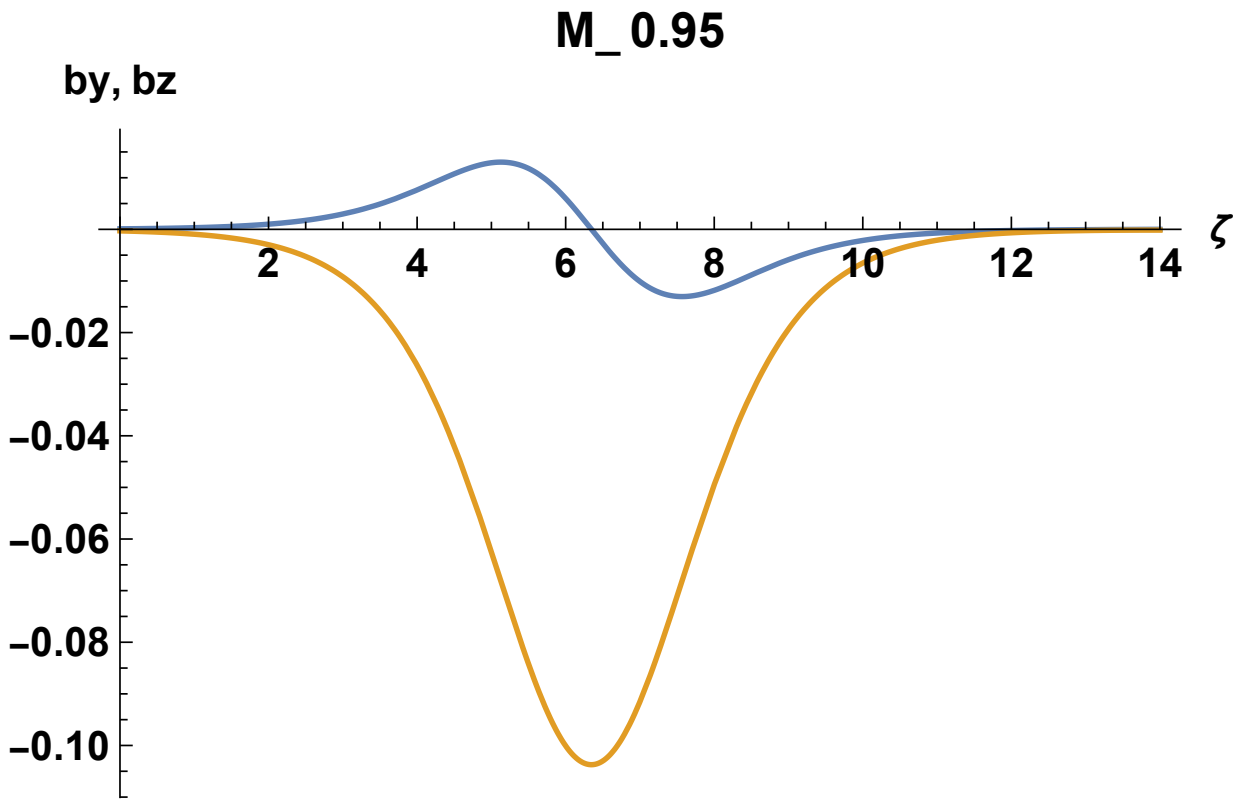

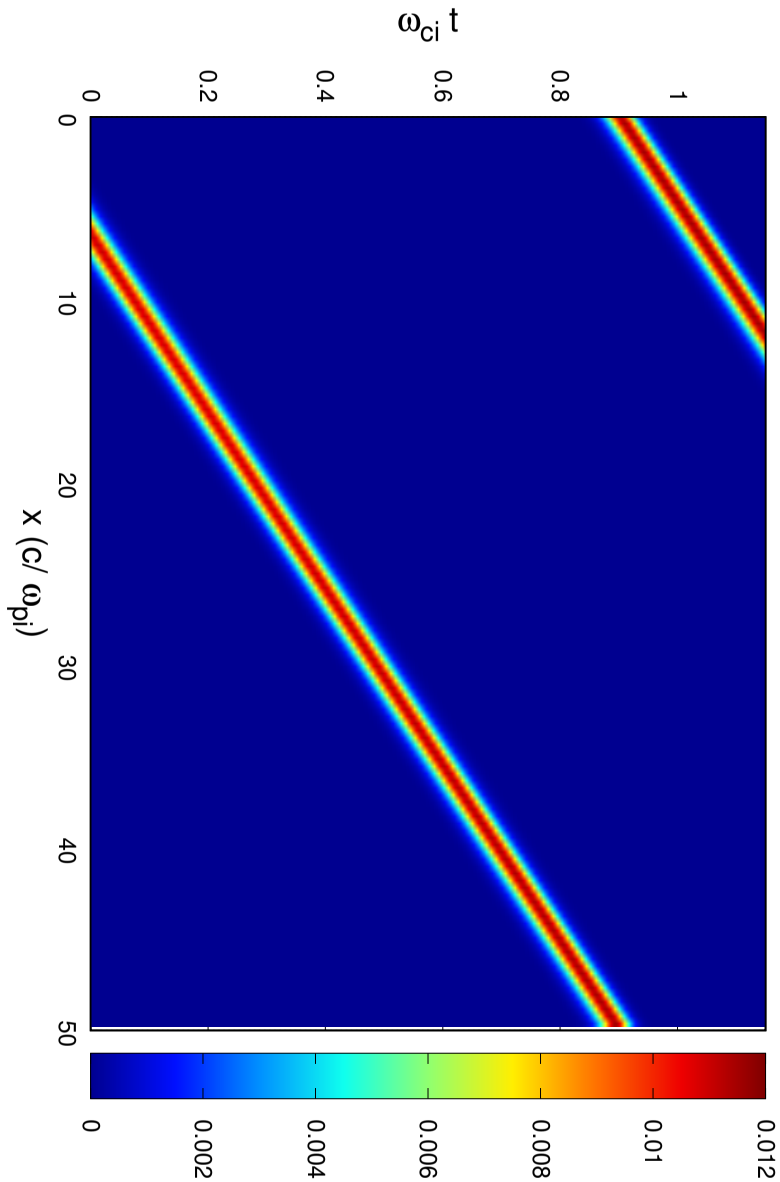

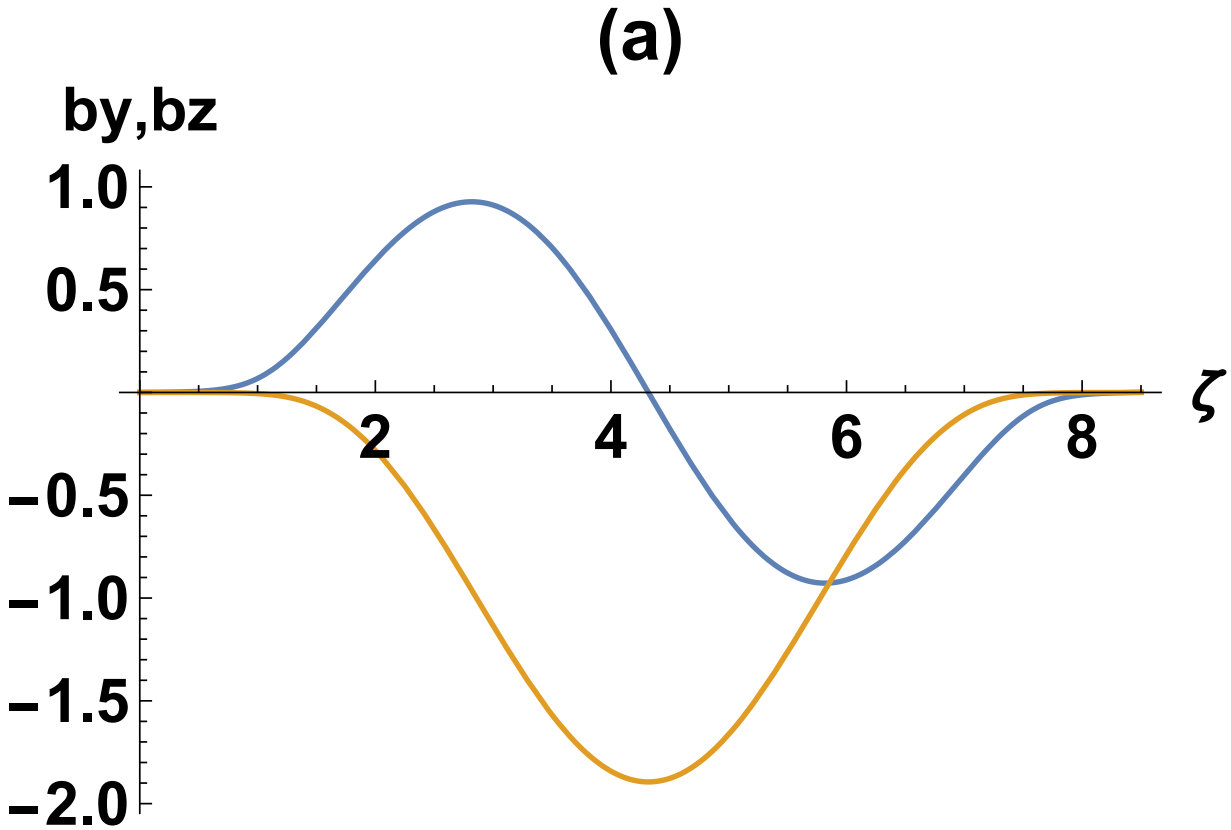

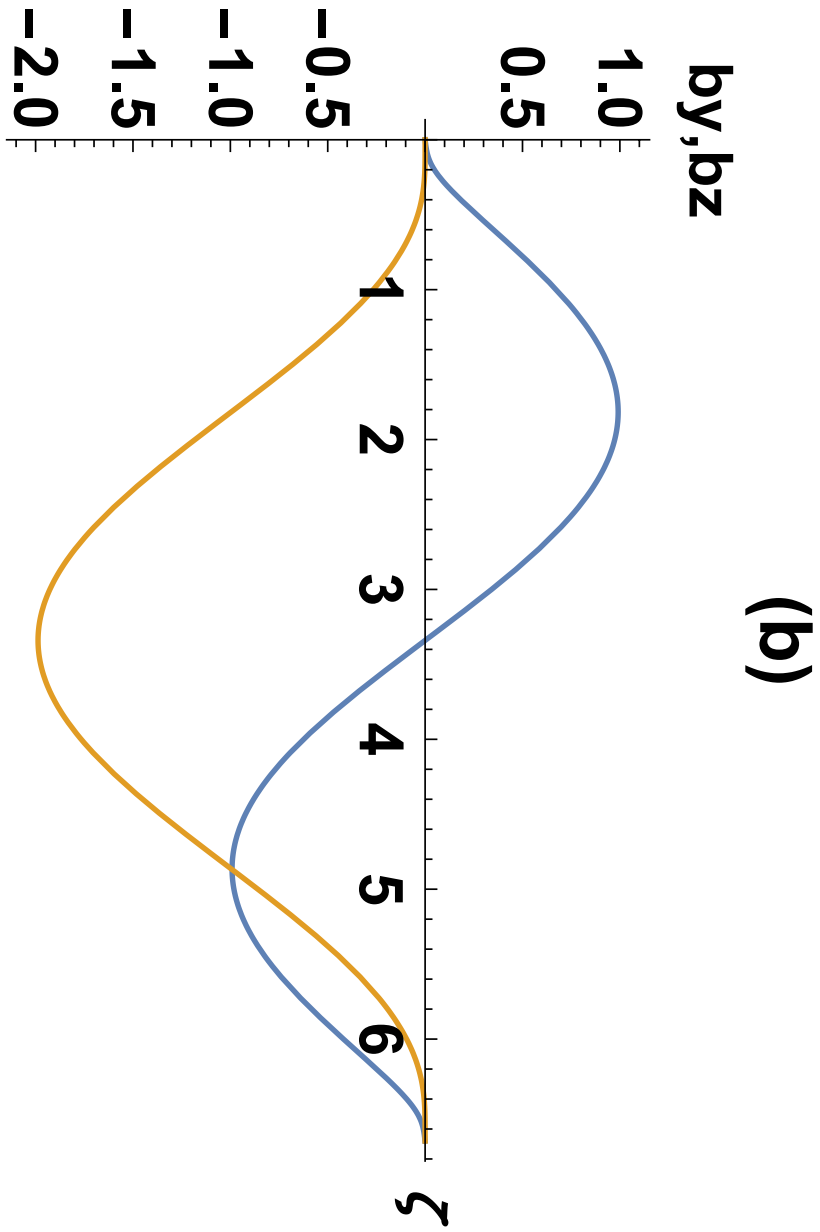

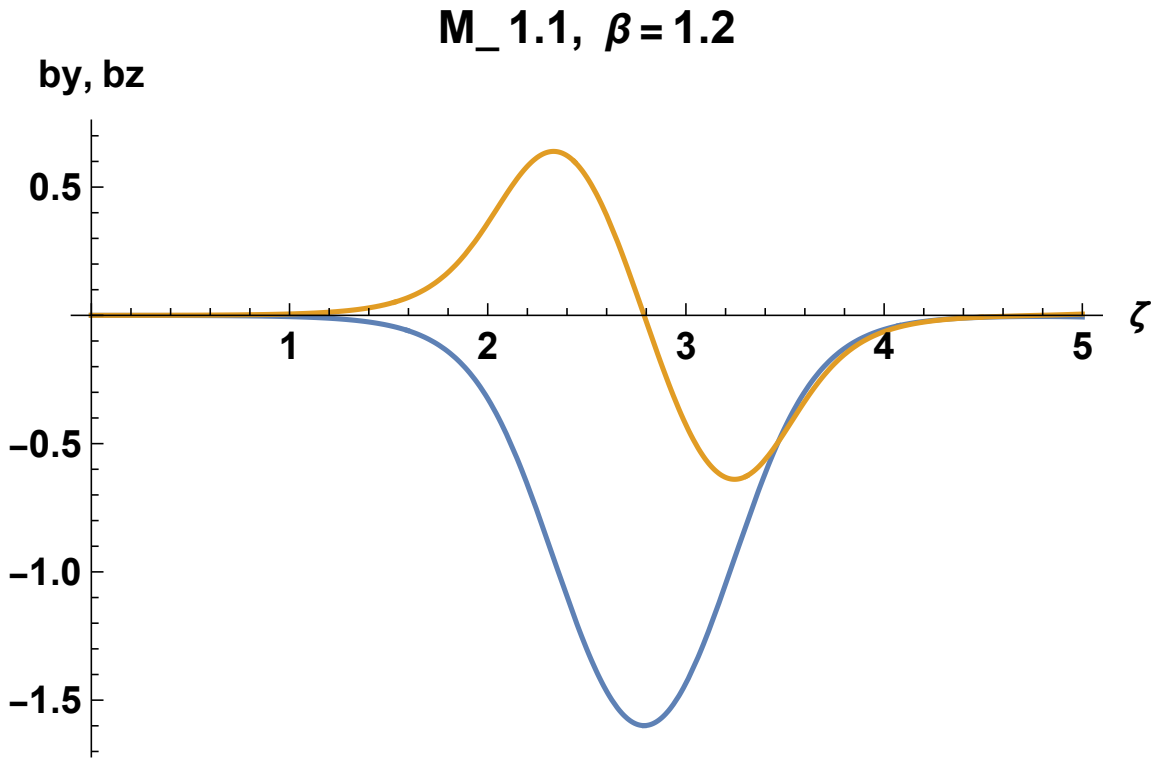

PLEASE CITE THIS ARTICLE AS DOI: 10.1063/5.0099201

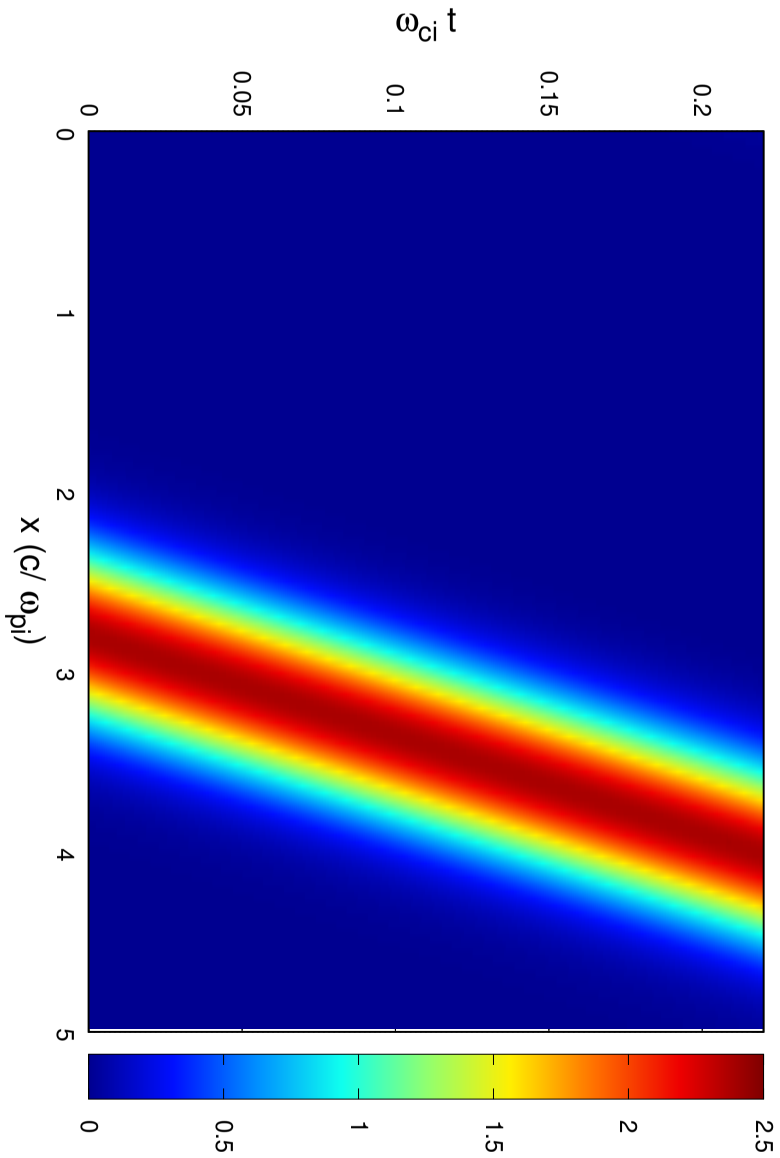

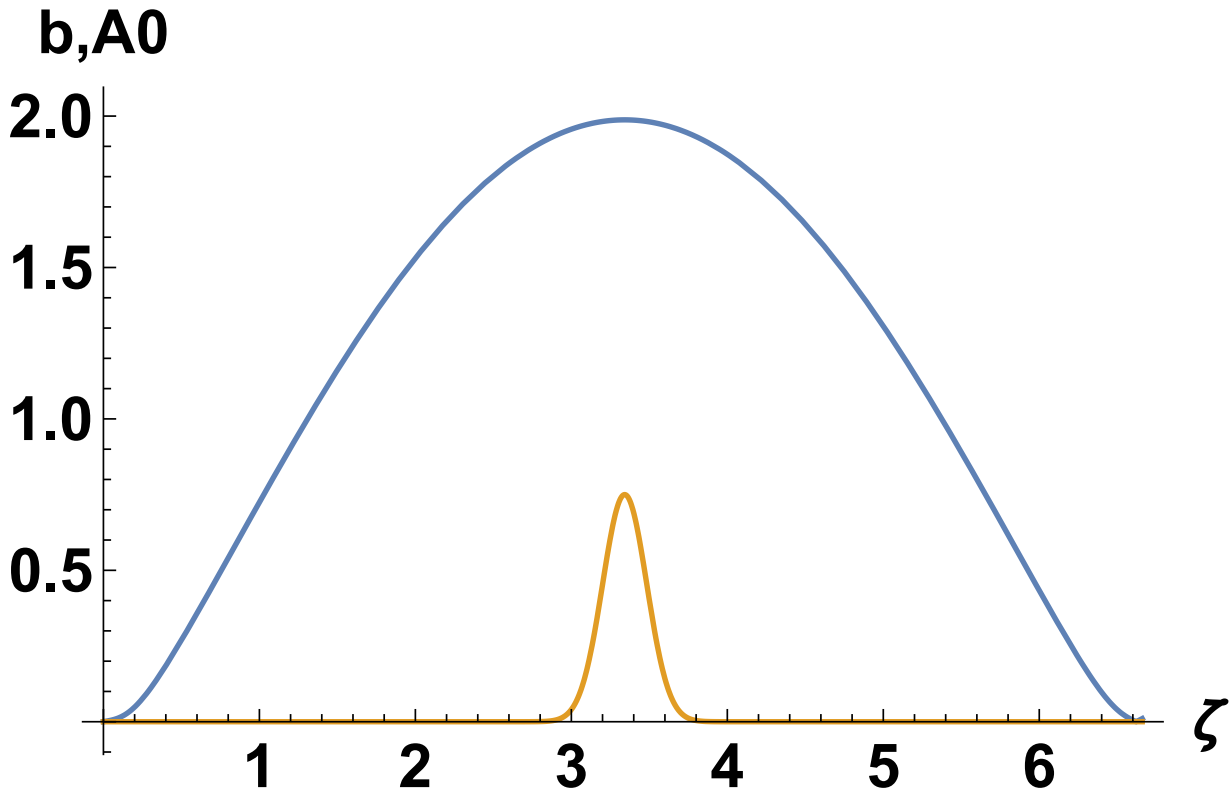

PLEASE CITE THIS ARTICLE AS DOI: 10.1063/5.0099201